# Synthesis and Photophysics of a 1-Pyrenyl Substituted 2′-Deoxyuridine-5-Carboxamide Nucleoside: Electron Transfer Products as CIS INDO/S Excited States

**Charles E. Kerr,[†] C. Denise Mitchell,[†] Jeb Headrick,[‡] Bruce E. Eaton,*[,‡] and Thomas L. Netzel*[,†]**

*Department of Chemistry, Georgia State University, Atlanta, Georgia 30303, and Department of Chemistry, Washington State University, Pullman, Washington 99164*

*Received: August 5, 1999; In Final Form: November 24, 1999*

This paper reports results of the synthesis and photophysical study of 5-(*N*-carboxy-1-aminopyrenyl)-2′-deoxyuridine (PA-dU) and its spectroscopic model *N*-acetyl-1-aminopyrene (PA-Ac). Absorbance and emission spectra, emission quantum yields, and emission lifetimes are reported for both compounds in three solvents. The data show that the emission yield quenching of PA-dU relative to PA-Ac varies from 95 to 99% in the solvent series THF, MeCN, and MeOH. In contrast to the monoexponential kinetics for $(\pi,\pi^*)^1$ emission from PA-Ac, the $(\pi,\pi^*)^1$ emission from the PA-dU nucleoside decays with two lifetimes in THF and three in MeCN and MeOH. The multiexponential emission decays are likely due to the presence of multiple nucleoside conformers. The average $(\pi,\pi^*)^1$ lifetimes for PA-dU in THF, MeCN, and MeOH are, respectively, 4.8, 2.7, and 0.55 ns and correspond to lifetime quenching values of 58, 81, and 96%, respectively. The lifetime quenching values for PA-dU in THF and MeCN do not agree with the emission yield quenching values in these solvents of, respectively, 95 and 96%. Thus in these two solvents the emitting states for PA-dU have lower radiative rates than do the emitting states for PA-Ac in the same solvents. However, for PA-dU in MeOH the lifetime quenching percentages of 96% over the 380−440 nm range and 98% over the 405−440 nm range are in good agreement with the emission yield quenching value of 99% in this solvent. Additionally, the emission spectrum of PA-dU in MeOH matches the $(\pi,\pi^*)$ emission spectrum of PA-Ac in MeOH, while the emission spectra of PA-dU in THF and MeCN do not match the corresponding spectra of PA-Ac. Thus choice of solvent tunes the electronic nature and the radiative rate of the emitting state in PA-dU. Emission quenching in PA-dU is assigned to intramolecular electron transfer (ET), and the 550−600 nm emission region of PA-dU reflects the relaxation dynamics of the pyrene$^{\bullet+}$/dU$^{\bullet-}$ ET product. Strikingly emission lifetimes in this spectral region in all three solvents are extremely short, ≤100 ps. CIS INDO/S computations of the excited states for the 5-(*N*-carboxy-1-aminopyrenyl)-1-methyluracil (PA-$U_{Me}$) model show that two factors are major contributors to the variation in ET product ($ET_1$) energy among the eleven PA-$U_{Me}$ conformers identified. The first is the energy of the uracil LUMO (a redox effect), and the second is the pyrenyl/$U_{Me}$ subunit separation distance (a Coulombic effect). Importantly, the dihedral angle between the bridging carbonyl and the C5−C4 bond in $U_{Me}$ is strongly correlated with the energy of the uracil LUMO ($R = 0.94$) and thus with the $ET_1$ energy. Finally, quantitative study of the energy of the $ET_1$ state versus pyrenyl/$U_{Me}$ separation distance shows a smooth $x^{-1}$ increase in $ET_1$ energy as the separation distance increases ($R = 0.9994$). Additionally, the extrapolated $ET_1$ energy at infinite subunit separation equals the difference between the LUMO and HOMO energies.

## Introduction

In recent years a number of measurements of DNA-mediated electron transfer (ET) have been reported, and this work has also been reviewed several times.[1−3] Progress is occurring,[4−10] but it is still unclear whether the distance dependence of ET in DNA is always strong or can under some circumstances be quite shallow.[11−16] Recent cation migration studies by Giese et al.[4,5] and Schuster et al.[17] investigated the distance dependence of the cation migration indirectly from strand-cleavage assays. Such studies provide important information concerning the distance dependence of hole tunneling and hole hopping in DNA, reinforcing the need for direct rate measurements of these reactions.

Our approach to studying charge migration in DNA focuses on examining the motion of a photoproduced 2′-deoxyuridine anion (dU$^{\bullet-}$) that can migrate to covalently attached electron acceptor sites.[18] These experiments are designed to measure directly the kinetics of electron migration in DNA by means of laser-flash transient absorbance (TA) spectroscopy. To understand the structural effects of dU$^{\bullet-}$ photoproduction in DNA, we have synthesized and studied the photophysics of ET in a family of pyrenyl-dU nucleosides.[19,20] Our earlier work in this area showed that indeed photoinduced electron transfer (ET) did occur in ≤30 ps to form the pyrene$^{\bullet+}$/dU$^{\bullet-}$ ET product. However, the longest lifetimes observed for this product were 100 ps in acetonitrile (MeCN) and 70 ps in methanol (MeOH).[20]

An important first step in measuring the above-described motion in DNA requires trapping an excess electron on deoxyuridine long enough to allow it time to travel to other DNA sites. The competing reaction, of course, is back ET

* To whom correspondence should be addressed. Department of Chemistry, Georgia State University Atlanta, GA 30303.
[†] Department of Chemistry, Georgia State University.
[‡] Department of Chemistry, Washington State University.

10.1021/jp992773j CCC: $19.00 
Published on Web 02/02/2000

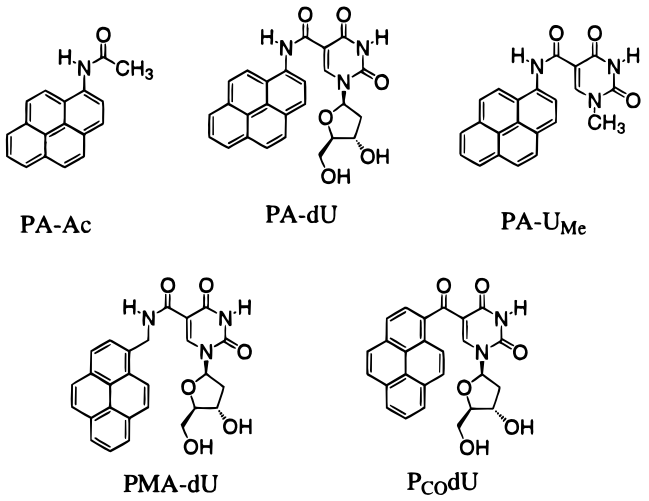


**Figure 1.** Structural drawings of the pyrenyl ligand model *N*-acetyl-1-aminopyrene (PA-Ac), *N*-(1-pyrenyl)-2′-deoxyuridine-5-carboxamide (PA-dU), the computational model *N*-(1-pyrenyl)-1-methyluracil-5-carboxamide (PA-U$_{Me}$), and two other pyrene-deoxyuridine nucleosides: *N*-(1-pyrenylmethyl)-2′-deoxyuridine-5-carboxamide (PMA-dU) and 5-(1-pyrenylcarbonyl)-2′-deoxyuridine (P$_{CO}$dU).

**SCHEME 1**

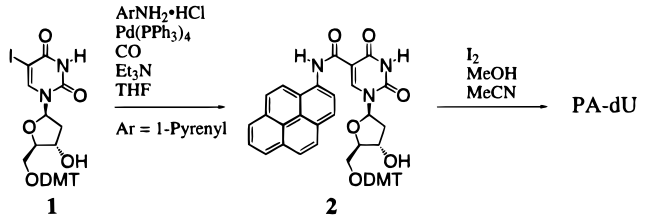


between the photooxidized pyrenyl ligand (pyrene$^{\bullet+}$) and the initially reduced deoxyuridine nucleoside. One way of doing this is to make the covalent linker that joins the pyrenyl and deoxyuridine subunits of the right length and composition. This would allow the photoinduced charge separation event (formation of pyrene$^{\bullet+}$/dU$^{\bullet-}$) to be ca. 99% efficient and the back (or reverse) ET reaction to be slow enough to allow the electron on the reduced deoxyuridine to transfer to other DNA sites. A practical variation on this theme involves the use of a secondary electron donor to reduce the pyrene$^{\bullet+}$ ligand and thereby extend the lifetime of the trapped deoxyuridine anion.

With these considerations in mind, we present in this paper the results of our synthesis and photophysical study of the 5-(*N*-carboxy-1-aminopyrenyl)-dU nucleoside (PA-dU, see Figure 1). Our immediate goal in these studies is to learn about the intrinsic forward and reverse ET processes in this nucleoside as a means of developing pyrenyl-dU nucleosides with ET product lifetimes in the ca. 0.5 ns time range. Additionally this paper presents the results of CIS INDO/S theoretical computations of the excited-state properties of a variety of conformers of the 5-(*N*-carboxy-1-aminopyrenyl)-1-methyluracil nucleoside model (PA-U$_{Me}$). Taken together these investigations identify key factors that control the energy and properties of pyrene$^{\bullet+}$/dU$^{\bullet-}$ ET products. These include redox and molecular orbital shape effects due to substitutent orientation on donor/acceptor (D/A) subunits and Coulombic interactions within the ET product.

## Materials and Experimental Methods

**General Synthetic Methods.** Deoxyuridine analogs were prepared by adaptation of previously published procedures.[21] All palladium coupling reactions (Scheme 1) were conducted in a glass coupling apparatus equipped with teflon stopcocks. Reagents and solvents for palladium coupling reactions were prepared to be air and moisture free and then were stored and combined in a Vacuum Atmospheres, Inc., glovebox (argon or nitrogen atmosphere). Reactions conducted outside the glovebox were performed under an argon or nitrogen atmosphere. Tetrahdrofuran (THF) was distilled from benzophenone Na/K alloy and stored with rigorous exclusion of moisture and oxygen. Triethylamine (Et$_3$N) and acetonitrile (MeCN) were purified by distillation from calcium hydride under inert atmosphere, and methanol (MeOH) was dried by distillation from magnesium turnings under an inert atmosphere. Whatman brand (80 Å pore, 230−400 mesh) silica gel and Biotage KP−Sil cartridges were used for column chromatography. NMR data were acquired on Bruker and Varian spectrometers ($^1$H 300 MHz) at the WSU NMRSC and at GSU. Mass spectral data were obtained from facilities at Washington State University and The Georgia Institute of Technology.

**Preparation of *N*-Acetyl-1-aminopyrene (PA-Ac).** Pyridine (40 mL), 1-aminopyrene (0.5 g, 2.3 mmol), and acetic anhydride (12 mL) were combined and stirred at 50 °C for about 18 h. After drying in vacuo, the product was recrystallized from acetone as fine white needles (0.37 g, 1.4 mmol, 62%). Mp (uncorrected) 265−267 °C melts/decomposes. $^1$H NMR (300 MHz: DMSO-$d_6$) $\delta$ 2.28 (s, 3H), 8.18 (arom., 9H), 10.33 (s, 1H); $^{13}$C {$^1$H} (75 MHz: DMSO-$d_6$) $\delta$ 15.45, 114.06, 114.97, 115.33, 115.60, 116.05, 116.54, 116.62, 116.86, 118.05, 118.16, 118.66, 118.92, 119.76, 122.17, 122.52, 123.71, 160.71. MS (EI+) *m*/*z* for $C_{18}H_{13}NO$ ($M^+$) Calcd 259.0997. Found 259.0989.

**Preparation of *N*-(1-Pyrenyl)-5′-*O*-dimethoxytrityl-2′-deoxyuridine-5-carboxamide (2).** A Pyrex high-pressure bomb was transferred to an inert atmosphere glovebox and charged with 1-(2′-deoxy-5′-dimethoxytrityl-$\beta$-D-ribofuranosyl)-5-iodouracil (**1**) (154 mg, 0.235 mmol), 1-aminopyrene (168 mg, 0.773 mmol) tetrakis(triphenylphosphine)palladium(0) (55 mg, 48 $\mu$mol), THF (2.4 mL), and Et$_3$N (600 $\mu$L). The Teflon stopcock was closed, and the bomb removed from the box and charged with CO (nominal 50 psig). The reaction vessel was then heated in an oil bath (70 °C) for approximately 20 h. The bomb was then cooled, recharged with CO, and heated again until a total of 5 days had elapsed. The crude mixture was rinsed from the reaction vessel using acetone and MeOH, concentrated, and purified on a Biotage Flash 12 M KP−Sil column using a stepped eluant series (methylene chloride containing trace Et$_3$N; 1% MeOH/$CH_2Cl_2$; 2.5% MeOH/$CH_2Cl_2$; 5% MeOH/$CH_2Cl_2$). Concentration of the appropriate fractions gave **2** (149 mg, 0.193 mmol, 82.3%) as a greenish-yellow solid. MS (FAB) *m*/*z* for $C_{47}H_{39}N_3O_8$ ($M^+$) Calcd 773.274. Found 773. $^1$H and $^{13}$C NMR are not given for these structures since the large number of overlapping aromatic peaks makes assignment in this region unconvincing. However, a partial analysis of the $^1$H NMR spectrum was made to verify the presence of the deoxyribosyl moiety.

**Preparation of *N*-(1-Pyrenyl)-2′-deoxyuridine-5-carboxamide (PA-dU).** Removal of the 5′-DMT protecting group was accomplished as previously reported.[22] Compound **2** (156 mg, 0.202 mmol) was dissolved at 65 °C in dry MeOH (30 mL) and dry MeCN (10 mL) in a flask under nitrogen. Iodine (400 mg, 1.58 mmol) was added, and the flask was placed in a 60−50 °C oil bath and the contents stirred. Reaction progress was followed by silica gel TLC (mobile phase: 10% MeOH/$CH_2Cl_2$). The reaction was quenched in 20 min by addition of aqueous sodium bisulfite. To this solution was added flash silica (2 g) and the mixture concentrated under reduced pressure,

followed by coevaporation with MeOH and acetone.[22] The dried residue was chromatographed on a Biotage Flash 12 M KP−Sil column using first 5% MeOH/$CH_2Cl_2$ then 20% MeOH/$CH_2Cl_2$. After concentration of the eluate, the solid was washed with water, and recrystallized (MeOH/$CH_2Cl_2$). Further purification steps included washing the crystals with methylene chloride and then MeOH, followed by recrystallizing from MeOH by ether diffusion. The free nucleoside PA-dU (43 mg, 0.091 mmol, 45%) was obtained as a yellowish green powder. $^1$H NMR (300 MHz: DMF-$d_7$) $\delta$ 2.43 (m, 2H, $H_{2'\alpha}/H_{2'\beta}$), 3.83 (~dd, $J$ = 3.5, 7.7 Hz, 2H, $H_{5'\alpha}/H_{5'\beta}$), 4.09 (dd, $J$ = 3.4, 6.5 Hz, 1H, $H_{4'}$), 4.52 (~p, $J$ = 3.7 Hz, 1H, $H_{3'}$), 5.38 (t, $J$ = 4.5 Hz, 1H, $OH_{5'}$), 5.48 (d, $J$ = 4.1 Hz, 1H, $OH_{3'}$), 6.36 (t, $J$ = 6.6 Hz, 1H, $H_{1'}$), 8.12 (m, 3H, pyrene H's), 8.36 (m, 5H, pyrene H's), 9.07 (d, $J$ = 8.5 Hz, 1H), 9.24 (s, 1H, $H_6$), 12.11 (s, 1H, amide-NH), 12.36 (s, 1H, imide-$H_{N3}$). $^{13}$C {$^1$H} (75 MHz: DMSO-$d_6$) $\delta$ 40.66 ($C_{2'}$), 61.18 ($C_{5'}$), 70.41 ($C_{4'}$), 86.08 ($C_{3'}$), 88.16 ($C_{1'}$), 105.20, 119.58, 119.91, 120.73, 124.09, 124.42, 124.96, 125.46 (two resonances coincident), 126.23, 126.55, 127.37, 127.42, 127.97, 130.45, 131.04, 131.75, 147.08 ($C_5$), 149.58 ($C_6$), 160.43 ($C_4$), 164.37 ($C_2$). MS (EI+) $m/z$ for $C_{26}H_{21}N_3O_6$ (M+) Calcd 471.1430. Found 471.1445.

**UV-Vis Absorbance and Emission Spectroscopic Methods.** Absorbance spectra were recorded on a Shimadzu UV 2501PC high performance spectrophotometer equipped with a double monochromator for reduced stray light. The bandwidth for absorbance spectra was 1 nm, and sample concentrations were $(3.5-4.0) \times 10^{-5}$ M. Molar absorbance coefficients ($\epsilon$) for PA-Ac and PA-dU were measured in THF, MeCN, and MeOH. PA-Ac or PA-dU (1.1−1.9 mg) were weighed to ±0.01 mg and dissolved by stirring for 1 week in a 100 mL volumetric flask. Quantitative dilutions were made to produce Beer's law plots for $\epsilon$ calculation. For both compounds the molar absorbance coefficients were invariant among the three solvents studied. The $\epsilon$ values in MeOH for PA-Ac and PA-dU were, respectively, $25.7 \pm 0.9 \times 10^3$ M$^{-1}$ cm$^{-1}$ at 340 nm and $28.3 \pm 0.9 \times 10^3$ M$^{-1}$ cm$^{-1}$ at 358 nm.

Fluorescence spectra were recorded on an SLM-8000C (SLM Aminco, Inc.) spectrofluorometer and corrected for the spectral response of the optical system. The correction factors were determined at GSU using a standard lamp whose energy output was traceable to NIST calibrations. The corrected emission spectra reported in this paper are plotted as relative detected intensity versus wavelength. To eliminate nonisotropic emission polarization artifacts for both emission spectra and quantum yield measurements, a quartz achromatic depolarizer was placed in the excitation beam and the emission was recorded through a calcite polarizer set at 54.7° with respect to vertical.[23] This defined the polarization of the light in the emission detection system and allowed correction factors to be developed. The excitation wavelength for both emission spectra and quantum yield measurements was 341 nm. For emission spectra the excitation and emission bandwidths were 4 nm, and sample concentrations were $3.7-4.5 \times 10^{-6}$ M.

For emission quantum yield measurements ($\Phi_{em}$) for PA-Ac, the excitation and emission bandwidths were 2 nm, and the absorbances of the two samples (unknown and reference) being compared were made nearly identical at 341 nm at an absorbance value close to 0.1. The corrected emission area (integral of corrected emission quanta versus wavelength, $D_x$) for each sample was then directly measured. For $\Phi_{em}$ measurements for PA-dU, this was not possible because of the very weak emission for this nucleoside in all three solvents studied. Rather an indirect procedure for determining $D_x$ described by Parker and Rees was used.[24,25] This method assumed that the ratio of the corrected emission area to the uncorrected emission intensity at any convenient wavelength was not a function of the excitation intensity or bandwidth. Thus according to this method, $D_x$ was measured in two experiments. In one the ratio of emission area to uncorrected emission intensity at a selected wavelength was determined using broad excitation bandwidth (high intensity), while in a second experiment the uncorrected intensity at the selected wavelength alone was determined with 2-nm bandwidth. The product of the ratio defined above and the measured uncorrected intensity at the selected wavelength gave the corrected emission area ($D_x$) for 2-nm bandwidth excitation.

Emission quantum yields were calculated according to equation 1.[25]

$$\Phi_{em}^{x} = \Phi_{em}^{r}\left(\frac{D_x\eta_x^2}{A_x}\right)/\left(\frac{D_r\eta_r^2}{A_r}\right) \quad (1)$$

In Equation 1, $x$ and $r$ refer to the unknown and reference solutions, respectively; e.g., $D_x$ is the corrected emission area of the unknown solution; $A_x$ is the absorbance of the unknown solution at the exciting wavelength; and $\eta_x$ is the refractive index of the unknown solution.

For reference use the fluorescence quantum yield for deoxygenated 1-pyrenylbutanoic acid (PBA; Molecular Probes, Inc., High Purity Grade) in MeOH (spectroscopic or HPLC grade) was measured to be 0.065(2) relative to 9,10-diphenylanthracene (Aldrich, 98%) in cyclohexane (spectroscopic or HPLC grade, $\Phi_{em} = 1.00$).[26] The emission quantum yields of PA-Ac and PA-dU were subsequently measured relative to either deoxygenated or aerated PBA in MeOH ($\Phi_{em}$(aerated) = 0.0045(2)). To remove oxygen, solutions for emission spectra, quantum yield determinations, and emission lifetime measurements were bubbled with solvent-saturated argon. All PA-Ac and PA-dU samples were deoxygenated. The samples were contained in four-sided fluorescence cells (1-cm optical pathlengths) equipped with a valve (Teflon-to-glass seal) and a septum-sealed side arm. Solvent-saturated argon gas was introduced via a cannula through the septum and open valve to the bottom of the solution and vented through a second needle in the septum. After bubbling the solution for 30−45 min with magnetic stirring, the cannula was partially retracted, the valve closed, and the vent needle and cannula were removed from the septum. PBA emission in such a deoxygenated cell decreased due to oxygen diffusion and quenching less than 1% after 1 h. Emission measurements took less than 30 min.

**Fluorescence Lifetime Measurements.** Fluorescence decays were recorded on a Tektronix SCD1000 transient digitizer (≤0.35 ns rise time calculated from the bandwidth, ≤120-ps rise time for a step input 0.5 times the vertical range) and wavelength resolved with a 0.1-m double monochromator (Instruments SA, Inc. model DH10) in additive dispersion. Slits (2 mm) were used producing an 8-nm band-pass. The 1200-grooves/mm holographic gratings were blazed at 450 nm. After passing through the monochromator, the emission was detected with a Hamamatsu 1564U microchannel plate (200-ps rise time) for short emission lifetimes or a Hamamatsu 928 photomultiplier (2.2-ns rise time) for long ones. The excitation and emission beams were oriented at 90 degrees with respect to each other, and emission was detected through a Glan-Thompson polarizer set at 54.7° ("magic angle") with respect to vertical to eliminate artifacts due to rotational diffusion.[23] Additionally, emission was excited at 355 nm with the third harmonic of an active-

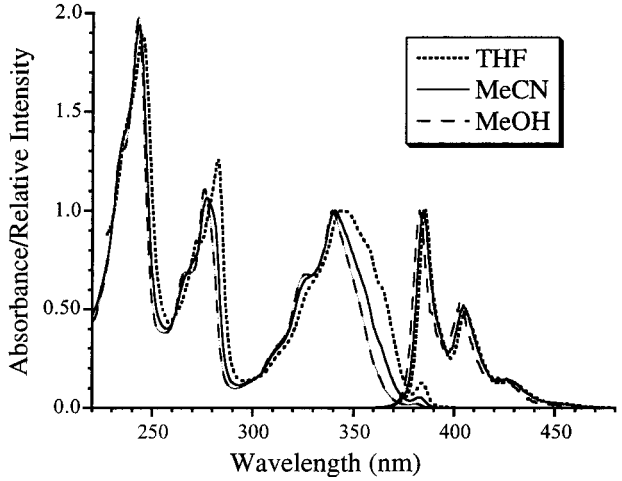


**Figure 2.** Absorbance and normalized emission spectra for the PA-Ac ligand model in three solvents. The sample concentrations for absorbance measurements in 1.0-cm path length cells were $4.03 \times 10^{-5}$, $3.98 \times 10^{-5}$, and $3.89 \times 10^{-5}$ M, respectively, in THF, MeCN, and MeOH; for emission measurements the concentrations were $3.7-4.0 \times 10^{-6}$ M.

passive mode-locked $Nd^{3+}$/YAG laser manufactured by Continuum, Inc. Typically 35-$\mu$J excitation pulses of ca. 25-ps duration were collimated into a 3-mm diameter beam and passed through a second Glan-Thompson polarizer set to vertical before entering the sample cuvette. Sample concentrations were adjusted so that the absorbance at 355 nm was 0.13−0.16 in a 1-cm cell, and their absorbance spectra were measured before and after lifetime measurements to verify that no decomposition occurred during these measurements. Photon Technology Incorporated software was modified by the manufacturer to process 1000 data points per decay curve and was used to deconvolute the instrument response from the emission decay to yield exponential lifetime fits to the emission decay data.

The temporal resolution of the emission kinetics system for multiexponential emission decays is generally ca. 0.2 ns; however, for nearly single-exponential decays it can be as good as ca. 50 ps after deconvolution.[19,20] A full description of the lifetime fitting procedure used here is presented in a paper by Netzel et al.[19] Included there are nine sets of emission decays on four time scales (20, 50, 100, and 500 ns) along with the following information: the equations used; plots of residual differences between experimental emission decays and calculated multiexponential curves; linear and logarithmic plots of emission decays, lamp decays and exponential curves; as well as specific $\chi_r^2$ values (the reduced chi-square statistic) for the plotted curves.

## Results

**UV-Vis Absorbance and Emission Spectra for PA-Ac and PA-dU.** Figure 2 presents plots of the absorbance and normalized emission spectra for the PA-Ac ligand model in THF, MeCN, and MeOH. The emission spectra in all three solvents are remarkably similar with the origin in MeOH at the shortest wavelength (383 nm) followed by MeCN (384 nm) and THF (385 nm). The absorbance spectra of PA-Ac in the two polar solvents, MeCN and MeOH, are nearly identical. Interestingly in THF the absorbance origins of PA-Ac in the 260−400-nm range are red-shifted 3−7 nm relative to their values in MeOH. This has the consequence that the molar absorptivity ($\epsilon$) of the first excited electronic state $S_1$ is largest in THF and decreases steadily as the solvent is varied from THF to MeCN and finally

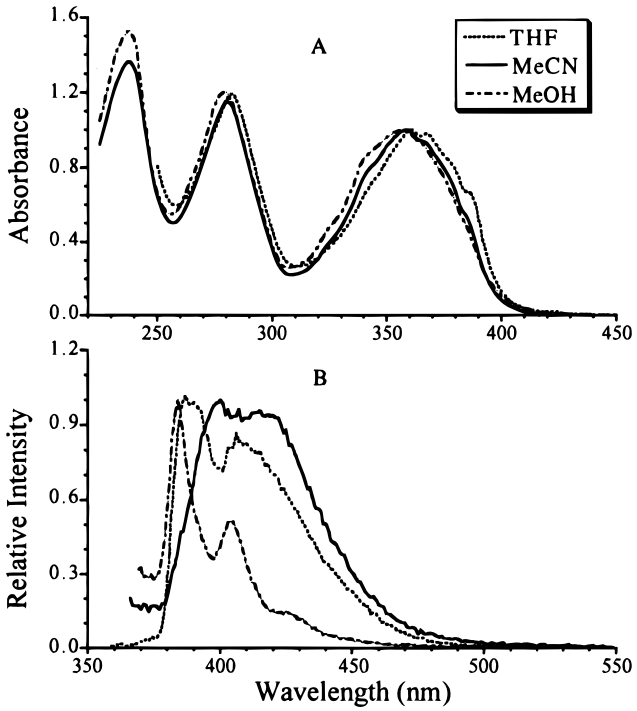


**Figure 3.** Absorbance (*A*) and normalized emission (*B*) spectra for the PA-dU nucleoside in three solvents. The sample concentrations for absorbance measurements in 1.0-cm path length cells were $3.64 \times 10^{-5}$, $3.50 \times 10^{-5}$, and $3.53 \times 10^{-5}$ M, respectively, in THF, MeCN, and MeOH; for the emission measurements the concentrations were $(4.2-4.5) \times 10^{-6}$ M.

to MeOH. Vibrational progression shoulders extending to short wavelength are apparent in the absorbance spectra of PA-Ac in all three solvents for each of the strong absorbance peaks. In emission a 1300-$cm^{-1}$ progression is clearly identifiable.

Note that in MeCN the origin of the $S_1(0,0)$ state is at 384 nm (3.23 eV); this electric dipole transition is spin-allowed, but orbitally forbidden. Two strongly allowed electronic origins are also apparent at 340 nm (3.65 eV) and 277 nm (4.48 eV). These electronic (0,0) positions in PA-Ac are nearly the same as in 1-alkyl pyrenes[19,27] and are useful excited-state markers for comparison with the theoretical excited-state computations (see below).

Figure 3 presents plots of the absorbance (*A*) and normalized emission (*B*) spectra for the PA-dU nucleoside in THF, MeCN, and MeOH. A striking observation is that absorbance spectra for PA-dU in all three solvents are much broader than for the pyrenyl model PA-Ac; thus the barley observable vibrational structure present in PA-Ac is washed out in the nucleoside. Aside from the 2-nm red-shift of the spectra in THF relative to MeCN and MeOH, the absorbance spectra of PA-dU are remarkably similar in all three solvents. The much broader, and significantly red-shifted absorbance spectrum for PA-dU compared to PA-Ac is direct evidence that the pyrenyl and uracil subunits in the nucleoside have strong electronic communication with each other. The emission origin is difficult to locate for PA-dU in THF and MeCN, but it appears to be close to 384 nm in MeOH. Also the broad emission spectra for PA-dU in THF and MeCN correspond reasonably with the broad absorbance spectra chararcteristic of PA-dU in all three solvents. The sharp vibrational features for PA-dU in MeOH are identical to those for PA-Ac in the same solvent, e.g., emission origins of 384 nm and 383 nm, respectively, for PA-dU and PA-Ac. One way of accounting for pyrenyl-type emission from PA-dU in MeOH would be to propose that some conformers for this

**TABLE 1: Emission Quantum Yield and Relative Emission Quenching in Three Solvents**

| compound | solvent | $\Phi_{em} \times 10^{3,a}$ | relative quenching[b] |
|---|---|---|---|
| PA-Ac | THF | 39(1) | |
| | MeCN | 26(1) | |
| | MeOH | 12(1) | |
| PA-dU | THF | 1.80(9) | 95.4(3)% |
| | MeCN | 0.97(5) | 96.3(3)% |
| | MeOH | 0.075(12) | 99.4(2)% |

[a] (±error). $\Phi_{em}$ measured relative to deoxygenated PBA in MeOH, $\Phi_{em} = 65(2) \times 10^{-3}$. [b] Relative Quenching $= [1 - \Phi_{em}(\text{PA-dU})/\Phi_{em}(\text{PA-Ac})] \times 100\%$.

**TABLE 2: Emission Lifetimes and Radiative Rates for PA-Ac and PBA**

| compound | solvent | $\tau$(ns)[a] | $k_{rad} \times 10^{-5}$, $s^{-1}$ |
|---|---|---|---|
| PA-Ac | THF | 11.3(0.2) | 34.5(1.5) |
| | MeCN | 14.2(0.2) | 18.3(0.9) |
| | MeOH | 13.2(0.1) | 9.1(1.4) |
| PBA | MeOH | 219(1) | 3.0(0.1) |

[a] (±error). Only one emission lifetime ($\tau$) was observed in each solvent, and it was independent of observation wavelength. Reduced chi square ($\chi_r^2$) values for the lifetime fits were generally in the range 1.5−4.0. A 25-ps laser pulse at 355-nm wavelength excited the sample.

nucleoside have relative geometries that do not permit ultrafast ET between the pyrenyl and uracil subunits. However, this must be a small fraction of conformers since conformers lacking vibrationally resolved spectral features dominate the absorbance spectrum. Emission from this majority of conformers with strong subunit interaction is totally quenched.

**Emission Quantum Yields for PA-Ac and PA-dU.** Table 1 lists the emission quantum yields ($\Phi_{em}$) for PA-Ac and PA-dU in three solvents and the relative quenching of the emission in the nucleoside relative to PMA-Ac in each solvent. These data show that the emission quenching varies from 95 to 99% in the solvent series THF, MeCN, and MeOH. Indeed in MeOH the nucleoside has less than 1% of the emission of the PA-Ac ligand model.

**PA-Ac Emission Lifetimes and Radiative Rates.** Table 2 lists emission lifetimes ($\tau$) and corresponding radiative rates ($k_{rad} = \Phi_{em}/\tau$) for PA-Ac in three solvents and for PBA in MeOH. As expected from the decreasing molar absorptivity of the $S_0 \rightarrow S_1$ transition PA-Ac in the solvent series THF, MeCN, and MeOH, the radiative rate for PA-Ac in this series also decreases steadily as the solvent changes from nonpolar, to polar nonprotic, and finally to polar protic. In fact in MeOH the radiative rate for PA-Ac is only three times greater than that for PBA. Apparently solvent/solute interactions modify the electronic interaction between the carboxamido side chain and the pyrenyl chromophore. Note that the long fluorescence lifetime of PBA is a result of the forbidden character of its $S_0 \rightarrow S_1(\pi,\pi^*)$ absorption process. In contrast its strong absorbance maximum at 341 nm corresponds to a strongly allowed $S_0 \rightarrow S_2(\pi,\pi^*)$ optical transition. The carboxamido ligand of PA-Ac makes its $S_0 \rightarrow S_1$ optical transition in PA-Ac less forbidden than in PBA; additionally solvent/PA-Ac interactions tune this transition's oscillator strength.

**PA-dU Emission Lifetimes.** Figure 2 shows that the $(\pi,\pi^*)^1$ emission from the pyrenyl subunit of PA-Ac is prominent in the 380−440 nm range and relatively nonexistent above 475 nm. Figure 3 shows that this pattern is also true for PA-dU in MeOH. However, the emission from PA-dU in THF and MeCN extends beyond 500 nm to almost 550 nm. Table 3 reports that under conditions of laser excitation at 355 nm, emission from the PA-dU nucleoside can be seen as far as 600 nm in all three solvents. Similar long wavelength emission in other pyrenyl-substituted nucleosides has been reported previously and assigned to emission from a pyrene$^{\bullet+}$/dU$^{\bullet-}$ ET product.[19] Thus emission kinetics for pyrenyl-substituted nucleosides in the 380−440 nm region reflect primarily quenching of the pyrenyl $(\pi,\pi^*)^1$ state, while emission kinetics in the 550−600 nm region reflect primarily relaxation dynamics of the pyrene$^{\bullet+}$/dU$^{\bullet-}$ ET product.

**$(\pi,\pi^*)^1$ Emission Lifetimes in PA-dU.** In contrast to the monoexponential kinetics for $(\pi,\pi^*)^1$ emission from PA-Ac, the $(\pi,\pi^*)^1$ emission from the PA-dU nucleoside decays with two lifetimes in THF and three in MeCN and MeOH. The multiexponential emission decays are likely due to the presence of multiple nucleoside conformers. (This topic will be discussed again later in this paper.) Whether there are only a few conformers or a broad distribution of conformers with a few principle lifetimes cannot be determined from the data in Table 3. The effect of varying solvent on the $(\pi,\pi^*)^1$ emission kinetics can be judged in several ways. One is to calculate the average emission lifetimes ($\langle\tau\rangle$) in the 380−440 nm range along with their corresponding lifetime quenching values ($[1 - \langle\tau\rangle/\tau_0] \times 100\%$, where $\tau_0$ is the lifetime of PA-Ac in the same solvent). The average $(\pi,\pi^*)^1$ lifetimes for PA-dU in THF, MeCN, and MeOH are, respectively, 4.8, 2.7, and 0.55 ns and correspond to lifetime quenching values of 58, 81, and 96%, respectively. The lifetime quenching values for PA-dU in THF and MeCN do not agree with the emission yield quenching values given in Table 1, respectively, of 95 and 96%. Thus the emitting states for PA-dU in THF and MeCN have lower radiative rates than do the emitting states for PA-Ac in these two solvents. However, for PA-dU in MeOH the lifetime quenching percentage over the 405−440-nm range is 98%, and both the 96 and 98% lifetime quenching values for PA-dU in MeOH are in good agreement with the emission yield quenching value of 99% in this solvent. Additionally, the emission spectrum of PA-dU in MeOH matches the $(\pi,\pi^*)^1$ emission spectrum of PA-Ac in MeOH, while the emission spectra of PA-dU in THF and MeCN do not match the corresponding spectra of PA-Ac. Taken together these observations support the conclusion that the emitting state for PA-dU in THF and MeCN is electronically different from the $(\pi,\pi^*)^1$ emitting state for PA-dU in MeOH and for PA-Ac in all three solvents studied. This means that the choice of solvent tunes the radiative rate of the emitting $(\pi,\pi^*)^1$ state in PA-Ac and the electronic nature as well as the radiative rate of the emitting state in PA-dU.

**ET Product Emission Lifetimes for PA-dU.** The 550−600 nm regions in Table 3 provide information on the dynamics of the pyrene$^{\bullet+}$/dU$^{\bullet-}$ ET product. Strikingly these lifetimes in all three solvents are extremely short, ≤100 ps. Note also that the different solvent dependence of the emission lifetimes in the 380−440- and 550−600-nm regions accords with the assignment of different emitting species to these two spectral regions. These lifetime results suggest that it may be difficult to observe the ET product for PA-dU in any of these solvents via TA measurements with 30-ps time resolution. A key question concerning the pyrene$^{\bullet+}$/dU$^{\bullet-}$ ET product is, "Where is it located with respect to the energy of the pyrenyl subunit's lowest-energy $(\pi,\pi^*)^1$ state?" The ET product could be populated either directly by excitation at 355 nm or indirectly by decay of the lowest energy pyrenyl $(\pi,\pi^*)^1$ state. The answer likely varies with solvent. In MeOH conformers with a partially quenched pyrenyl $(\pi,\pi^*)^1$ state emit from 384 to 440 nm, while the ET product from at least some conformers emits in the 500−600-nm range. The dominant conformers with strong subunit

**TABLE 3: Emission Lifetimes (ns) for PA-dU in Three Solvents[a]**

| | λ (nm) | | | | | | |
|---|---|---|---|---|---|---|---|
| | 386 | 391 | 415 | 440 | 500 | 550 | 600 |
| THF | 0.9 ± 0.1 (54%)<br>8.0 ± 0.2 (46%) | 0.2 ± 0.1 (88%)[b]<br>7.1 ± 0.1 (12%) | 0.8 ± 0.1 (28%)<br>7.2 ± 0.1 (72%) | 0.8 ± 0.1 (31%)<br>6.7 ± 0.1 (69%) | ≤0.1 (98%)<br>6.4 ± 0.3 (2%) | ≤0.1 (99%)<br>6.3 ± 0.4 (1%) | ≤0.1 (100%) |
| | λ (nm) | | | | | | |
| | 400 | 415 | 440 | 500 | 550 | 600 | |
| MeCN | ≤0.1 (98%)[b]<br>3.2 ± 0.2 (1%)<br>10.3 ± 0.2 (1%) | 0.7 ± 0.2 (67%)<br>4.6 ± 1.2 (23%)<br>12.7 ± 1.4 (10%) | 0.7 ± 0.4 (67%)<br>4.6 ± 0.3 (25%)<br>12 ± 2 (8%) | ≤0.1 (98%)<br>6.1 ± 0.4 (2%) | ≤0.1 (100%) | ≤0.1 (100%) | |
| | λ (nm) | | | | | | |
| | 384 | 405 | 440 | 500 | 550 | 600 | |
| MeOH | 0.3 ± 0.1 (92%)<br>4.8 ± 1.4 (5%)<br>23 ± 4 (3%) | 0.1 ± 0.1 (98%)<br>3.0 ± 0.4 (1%)<br>12.9 ± 0.5 (1%) | 0.1 ± 0.1 (98%)<br>4.2 ± 0.4 (1%)<br>7.1 ± 0.5 (1%) | ≤0.1 (100%) | ≤0.1 (100%) | ≤0.1 (100%) | |

[a] (Lifetime relative amplitude %). Reduced chi square ($\chi_r^2$) values for the lifetime fits were in the range 2.0−3.5. A 25-ps laser pulse at 355-nm wavelength excited the sample. [b] Lifetime dominated by Raman scattering from the solvent.

**TABLE 4: ET Product Emission Lifetimes for PA-dU, $P_{CO}$dU, and PMA-dU in MeOH**

| nucleoside | lifetime (ns) | percent amplitude |
|---|---|---|
| PA-dU[a] | ≤0.1 | 100 |
| $P_{CO}$dU[b] | 0.4 ± 0.1 | 68 |
| | 1.8 ± 0.1 | 11 |
| | 7.2 ± 2 | 21 |
| PMA-dU[c] | 0.77 ± 0.05 | 65 |
| | 4.1 ± 0.1 | 33 |
| | 69 ± 2 | 2 |

[a] Emission kinetics at 500 nm. [b] Emission kinetics at 495 nm.[19] [c] Emission kinetics at 500 nm.[38]

interactions have a pyrenyl $(\pi,\pi^*)^1$ state that appears to be totally quenched due to ultrafast relaxation to a lower energy ET state. Thus in MeOH it seems that the ET product of PA-dU is below the lowest energy pyrenyl $(\pi,\pi^*)^1$ state.

**Comparison of ET Product Emission in PA-dU, $P_{CO}$dU, and PMA-dU.** Transient absorbance measurements for $P_{CO}$dU in MeOH found pyrene$^{\bullet+}$/dU$^{\bullet-}$ ET product formation in ≤30 ps. This product decayed with two lifetimes, 67 ps (90%) and 6 ns (10%).[20] The emission decay kinetics listed in Table 4 for this nucleoside are in good agreement with this transient absorbance result, bearing in mind the greater precision and signal-to-noise ratio of the emission kinetics data.[19] Comparing the emission decays at ca. 500 nm in MeOH for PA-dU, $P_{CO}$-dU, and PMA-dU in Table 4, shows that the primary ET product decays (i.e., in the <5-ns range) are the shortest in PA-dU (≤0.1 ns), of intermediate duration in $P_{CO}$dU (0.4−1.8 ns [79%]), and longest in PMA-dU [0.8−4.1 ns [98%]). The longest lifetime components possibly reflect slow ET product formation kinetics more than they reflect intrinsic ET product decay kinetics. Also, they comprise only 2−21% of the emission signal. Thus comparison of the emission decays of these three nucleosides in the 500−600-nm range suggests that while the pyrene$^{\bullet+}$/dU$^{\bullet-}$ ET product in PMA-dU lives significantly longer than the one observed in the $P_{CO}$dU nucleoside, the ET product in PA-dU lives a much shorter time.

**Computational Modeling of ET Product Energies in PA-$U_{Me}$.** *Computational Modeling Objectives.* Comparing the ET-product emission lifetimes in PA-dU to those in $P_{CO}$dU and PMA-dU suggests that the lifetime of the pyrene$^{\bullet+}$/dU$^{\bullet-}$ product is shortest in the PA-dU nucleoside. While it is encouraging that the shortest-lived ET products in PMA-dU appear to decay in the 0.5−1.0-ns time range, it is not encouraging that the ET product in PA-dU appears to live ≤100 ps. This means that it will likely be feasible for PMA-dU, but not for PA-dU, to use a secondary electron donor (e.g., a dialkylaniline also attached to DNA) to reduce the pyrenyl cation and thus trap reduced uracil for an extended period of time. A trapped uracil anion, as discussed above, is required for direct kinetics studies of the base sequence dependence of electron migration in DNA. Thus insight into the factors that control the lifetime of pyrene$^{\bullet+}$/dU$^{\bullet-}$ products in pyrenyl-substituted deoxyuridine nucleosides will likely be useful with respect to achieving this goal. In particular it is thus worth understanding why the ET product in PA-dU is so short-lived: in MeOH from 405 to 600 nm, across both the $(\pi,\pi^*)$ and ET product emission regions, 98% or more of the emission lives <200 ps. Observations of multiexponential $(\pi,\pi^*)$ emission decays in PA-dU are also related to this interest in controlling the lifetime of pyrene$^{\bullet+}$/dU$^{\bullet-}$ products. The multiple emission lifetimes evidence multiple PA-dU conformers during the lifetime of the excited state of pyrene. Thus it is natural to ask, "What conformers are likely to be present at the time PA-dU is photoexcited?" and "What are the relative energies of their pyrene$^{\bullet+}$/dU$^{\bullet-}$ ET product states?" The remainder of this paper reports the results of theoretical computations designed to address these two questions. Questions concerning the range of variation of D/A electronic coupling among PA-dU conformers and possible geometies of fully relaxed ET products in solvents with varying dielectic constants are not addressed here.

Although the experimental studies of photoinduced ET within the pyrenyl-labeled nucleosides take place in solution the best place to begin modeling the energetics of these conformers is in the gas phase. One reason is that the core electronic effects are present in the gas phase without the complications of approximate solution treatments. A second reason is that the solution phase results must be understood by comparison to the gas phase results. This paper discusses the results of gas phase computations of the ground and excited state properties of eleven pyrenyl-substituted uracil conformers. Three objectives of these gas phase computations are (1) to gain insight into the important geometries of likely ground-state nucleoside conformers, (2) to estimate the range of variation of their ET product energies, and (3) to understand the factors responsible for these energy variations. Accomplishing these objectives will likely suggest ways of improving pyrenyl-substituted deoxyuridine designs for use in DNA-mediated electron migration studies.

**TABLE 5: CIS INDO/S Results for five PA-$U_{Me}$ Conformers**

| conformer | amide bond geometry | relative heat of formation (eV) | CO/$U_{Me}$ dihedral angle[a] (deg) | C1-C5 distance[b] (Å) | C-to-C distance[c] (Å) | C7-N1 distance (Å) | $S_1(\pi,\pi^*)$ energy[e] (eV) | $S_1(\pi,\pi^*)$ dipole moment[e] (D) | $ET_1$ energy[f] (eV) | $ET_1$ dipole moment[f] (D) | uracil LUMO[g] (eV) |
|---|---|---|---|---|---|---|---|---|---|---|---|
| A | trans | 0.0000 | −163 | 3.83 | 7.89 | 11.96 | 3.77 | 3.39 | 3.80 | 16.6 | −0.85 |
| B | trans | 0.0747 | 145 | 3.83 | 7.87 | 11.43 | 3.75 | 4.01 | 4.17 | 20.6 | −0.75 |
| C | trans | 0.0835 | −130 | 3.82 | 7.98 | 11.37 | 3.77 | 3.00 | 4.30 | 28.5 | −0.67 |
| D | trans | 0.0859 | −161 | 3.81 | 7.97 | 11.52 | 3.77 | 2.54 | 3.98 | 15.1 | −0.82 |
| E | cis | 0.1154 | −84 | 2.94 | 5.42 | 7.54 | 3.76 | 6.04 | 4.42 | 23.5 | −0.44 |

[a] Dihedral angle between the linking carbonyl and the C5-C4 bond in 1-methyl uracil. [b] Distance from the pyrenyl C1-carbon to the C5-carbon on 1-methyuracil, bridge attachment positions. [c] Distance between the centers of the pyrenyl and 1-methyl uracil rings. [d] Distance between the pyrenyl C7-carbon and the N1-nitrogen on 1-methyl uracil, ring ends. [e] Lowest energy pyrenyl singlet excited state, $(\pi,\pi^*)^1$. [f] Lowest energy singlet ET state, $(\text{pyrene}^{\bullet+}/\text{UMe}^{\bullet-})^1$. [g] For all *trans*-conformers the uracil LUMO is the PA-$U_{Me}$ molecule's LUMO; however, for the *cis*-conformer **E** the uracil LUMO is actually the molecule's LUMO+1. Note that the pyrenyl HOMO energies are in the following ranges: −6.96 to −7.15 eV for the *trans*-conformers and −7.24 to −7.45 eV for the *cis*-conformers.

*The PA-$U_{Me}$ Compuational Model.* To emphasize pyrenyl-uracil interactions as well as to shorten computation times, PA-dU was modeled as 5-(*N*-carboxy-1-aminopyrenyl)-1-methyl uracil (PA-$U_{Me}$, see Figure 1). Also to shorten computation times and additionally to achieve good ground-state geometries, the semiempirical PM3 quantum mechanical method[27,28] was used for conformational searching. Spartan 5.1.1[30] provided a convenient Monte Carlo conformational search method based on randomly varying the angles of the three bonds linking pyrene to uridine. Each bond was randomly stepped in 60° increments yielding 218 ($=6^3$) possible initial conformations. These initial conformations were then energy minimized with PM3 and the resulting unique conformer geometries were saved. This search procedure produced eight conformers with a *trans*-amide bond (carbonyl and NH groups trans with respect to the C−N amido bond) and three with a *cis*-amide bond. [For the following discussion the "amide" term in references to *cis*-amide and *trans*-amide conformers will be dropped, i.e. all *cis*- and *trans*-conformer descriptions will refer to the amide bond.] Note that steric interactions constrain N-monosubstituted acetamides and alkylamides to *trans*-amide conformations (see additional discussion below).[31] Thus both PA-Ac and PA-dU are expected to be *trans*-amides. However, we have only indirect NMR evidence (see below) for this conformational assignment. Thus an additional question is of interest for excited-state computations to address. Is the range of ET product energies within the *trans*-family of PA-$U_{Me}$ conformers large enough to account for the ≤0.1−20-ns range of quenching lifetimes found for the PA-dU nucleosides?

*Conformer Heat of Formation Energies.* The relative heat of formation energies for the eight *trans*-conformers spanned the 0.000−0.088 eV range ($(0.0-3.5)k_BT$, where $k_B$ is the Boltzmann constant and $T = 298$ K), and the relative heat of formation energies for the three *cis*-conformers spanned the 0.095−0.115 eV range ($(3.8-4.6)k_BT$). As expected the *trans*-conformers were calculated to be lower in energy than the *cis*-conformers.

*Conformer ET Product Energies.* The conformer geometries found with Spartan 5.1.1 were transferred to HyperChem 5.1[32] where CIS[33] (configuration interaction with single-excitation determinants) INDO/S[34−36] (intermediate neglect of differential overlap approximate Hamiltonian with spectroscopically adjusted integral parameters) semiempirical computations of excited state properties were carried out. In this way vertical energies of the excited states (i.e. holding the ground state geometry constant) were determined. For the CIS computations, 10 HOMO and 10 LUMO orbitals were included. Increasing the number of these orbitals did not affect the energies of the lowest several, singlet excited states. Note that the INDO/S method has been parameterized to give reasonable agreement with experimental excited state energies. Since it is possible to use a dielectric continuum solvent model to "solvate" the vertical CIS excited states, but it is not possible to geometry optimize continuum-solvated excited states with available software, vertical energies are preferred for comparison with future studies of solvent effects on pyrenyl−uracil excited states. Additionally, the vertical excited state energies are probably sufficient to accomplish the above objectives.

The eight *trans*-conformers had lowest energy singlet ET product ($ET_1$) energies that spanned the 3.80−4.32 eV range, while the corresponding states for the three *cis*-conformers spanned the 4.27−4.42 eV range. Thus six out of eight *trans*-conformers had $ET_1$ excited states that were lower in energy than the lowest energy $ET_1$ state for the *cis*-conformers. It also appears that the range of $ET_1$ energies within the *trans*-family of conformers is large enough (ca. 0.5 eV) to be consistent with the observed range of $(\pi,\pi^*)^1$ emission decays due to varying ET quenching rates for different PA-dU conformers. It is important to recognize here that the range of energy for the lowest energy $(\pi,\pi^*)^1$ states arising from the pyrenyl subunit is 3.74−3.76 eV for all eleven PA-$U_{Me}$ conformers. Comparison of the $ET_1$ and lowest energy $(\pi,\pi^*)^1$ state energies shows that in the gas-phase all ET quenching reactions in PMA-$U_{Me}$ are endergonic by at least 0.03 eV. However, polar solvents can potentially lower the energy of ET product states more than they lower the energy of local $(\pi,\pi^*)^1$ states. Thus at least some of the PA-$U_{Me}$ conformers are expected to have exergonic ET quenching reactions in such solvents. Indeed, preliminary solution phase results for a dielectric continuum solvent similar to MeCN confirm the expected differential solvent stablization (energy lowering) of $ET_1$ states relative to local $(\pi,\pi^*)^1$ states for $ET_1$ states in PA-$U_{Me}$ conformers with sufficiently large dipole moments.

*Redox Effects on $ET_1$ State Energies.* The *trans*-PMA-$U_{Me}$ conformers can be grouped into two clusters based on their relative ground state energies: low energy (0.00−0.034 eV and high energy (0.75−0.12 eV). However there is little or no correlation of ET product energies with these two groupings: the $ET_1$ energies for the three conformers in the low energy group span the range 3.80−4.17 eV, while the $ET_1$ energies for the five conformers in the high energy group span the range 3.85−4.42 eV. It is true as noted above, however, that the *cis*-conformers have higher heats of formation than do the *trans*-conformers, and they also generally have higher $ET_1$ energies.

Table 5 presents computational results for five PA-$U_{Me}$ conformers. Five clear differences, typical of *cis*/*trans*-differences, can be seen between the data for *cis*-conformer E and those for the four *trans*-conformers in the table. In particular,

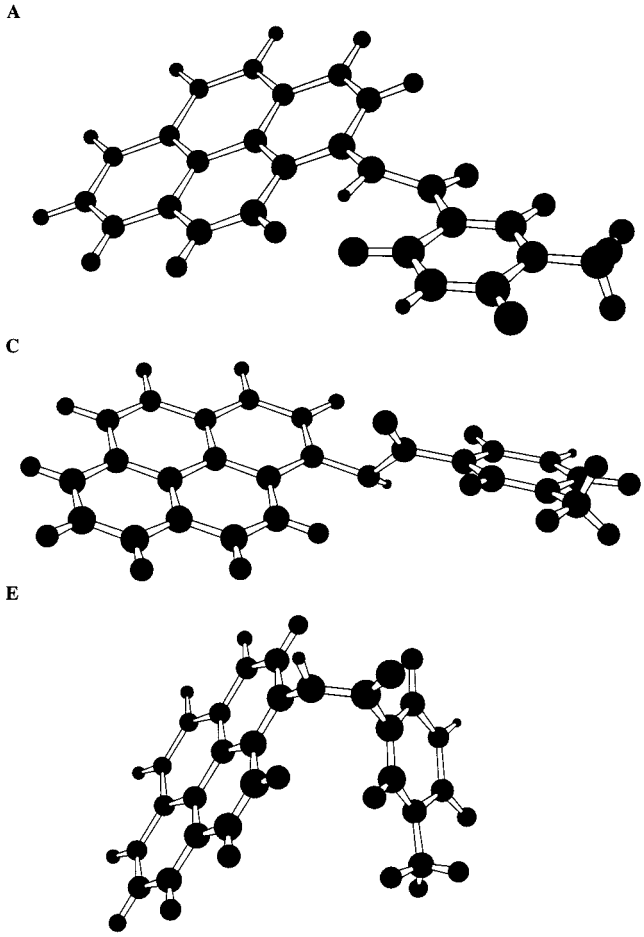


**Figure 4.** Ground state structures of PA-$U_{Me}$ conformers **A**, **C**, and **E** from Table 5.

(1) the CO/$U_{Me}$ dihedral angle is close to 90° for the *cis*-conformers and close to 180° for the *trans*-ones, (2) the pyrenyl and uracil subunits are much close together for the *cis*- than for the *trans*-conformers, (3) the dipole moment of the $S_1(\pi,\pi^*)$ state is larger for the *cis*- than for the *trans*-conformers, (4) the $ET_1$ energy is generally greater for the *cis*- than for the *trans*-conformers, and (5) the energy of the uracil LUMO is significantly higher (less negative) for the *cis*- than for the *trans*-conformers. Inspection of Table 5 suggests that the absolute value of the CO/$U_{Me}$ dihedral angle, the uracil LUMO energy, and $ET_1$ energy are correlated in PA-$U_{Me}$ conformers.

Figure 4 presents ball-and-stick structural models of the PA-$U_{Me}$ conformers **A**, **C**, and **E** from Table 5. Conformer **A** has the lowest heat of formation of all eleven conformers. It has a *trans*-amide bond, and its CO/$U_{Me}$ dihedral angle of −163° implies that its linking carbonyl bond is nearly in the plane of the uracil subunit. This conformer also has the lowest $ET_1$ energy (3.80 eV) only 0.03 eV above the energy of the $S_1(\pi,\pi^*)$ state. Conformer **C** also has a *trans*-amide bond, but its CO/$U_{Me}$ dihedral angle is −130°. This CO/$U_{Me}$ angle is the farthest away from the uracil plane among the eight *trans*-conformers and is responsible for the increasing the energy of the Uracil LUMO to −0.67 eV (the largest value among the eight *trans*-conformers). Not by chance the $ET_1$ energy of conformer **C** is nearly the largest among the *trans*-conformers (4.30 versus 4.32 eV for the largest one). Conformer **E** by way of contrast has a *cis*-amide bond. Figure 4 shows that its pyrenyl and uracil subunits face each other and form an A-frame (or clam) shaped structure. This explans why the distance measurements in Table 5 are substantially smaller for the *cis*- than for the *trans*-

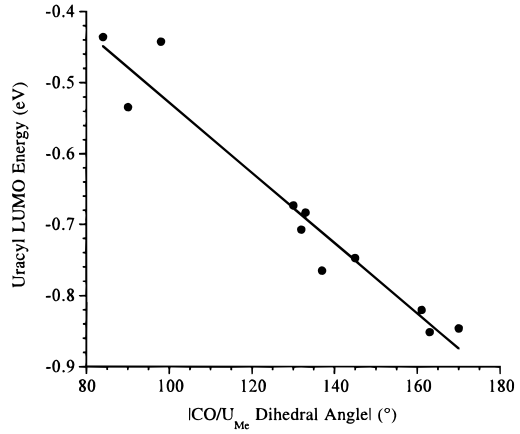


**Figure 5.** Linear least squares fit of energy of the Uracil LUMO in PA-$U_{Me}$ conformers versus the absolute value of their CO/UMe dihedral angle. See Table 5 for the CO/UMe dihedral angle definition. $R$ = 0.94.

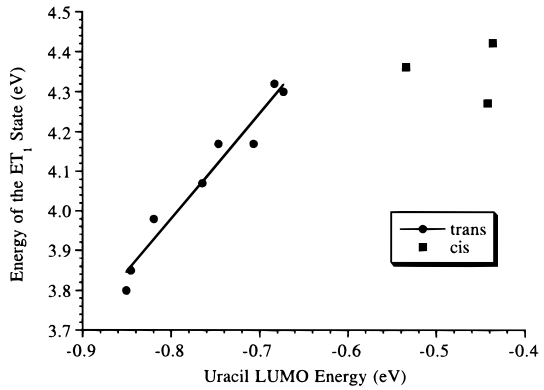


**Figure 6.** Plot of the energy of the $ET_1$ state in PA-$U_{Me}$ conformers versus the energy of their uracil LUMO: data for *trans*-conformers are shown in circles while data for *cis*-conformers are shown in squares. The linear least squares fit of the data for the *trans*-conformers has an $R$ value of 0.96.

conformers. It is important to note that the CO/$U_{Me}$ dihedral angle for conformer **E** is −84°. This implies that the linking carbonyl bond is nearly perpendicular to the plane of the uracil subunit, a feature common to all three *cis*-conformers. It is also interesting that the $ET_1$ dipole moment range for both the *cis*- and *trans*-conformers is nearly the same, 14.5−28.5 D, and that both sets of conformers have virtually the same $S_1(\pi,\pi^*)$ energy, 3.76(1) eV.

Figure 5 presents a plot of the energy of the uracil LUMO versus the absolute value of the CO/$U_{Me}$ dihedral angle for all eleven PA-$U_{Me}$ conformers. The correlation coefficient ($R$) is 0.94 indicating that there is a strong correlation between the CO/$U_{Me}$ dihedral angle and the energy of the uracil LUMO. The energy of this orbital in turn is a direct indicator of the ease of reduction of the uracil subunit. Thus when the CO group is nearly in the plane of the C4−C5 bond of $U_{Me}$, the uracil LUMO is low in energy and $U_{Me}$ is easy to reduce. When the CO group is out of the uracil plane, the uracil LUMO is high in energy, and $U_{Me}$ is more difficult to reduce.

*Coulombic Effects on $ET_1$ State Energies.* Figure 6 is a plot of the energy of $ET_1$ state versus the uracil subunit's LUMO energy in the eleven PA-$U_{Me}$ conformers. While there is an excellent correlation (R = 0.96) between these two parameters for *trans*-conformers, this correlation falls to 0.72 if data for both *cis*- and *trans*-conformers are included in the fit. Clearly there is at least another important contribution to $ET_1$ energy in addition to the location of the uracil LUMO. Comparison of

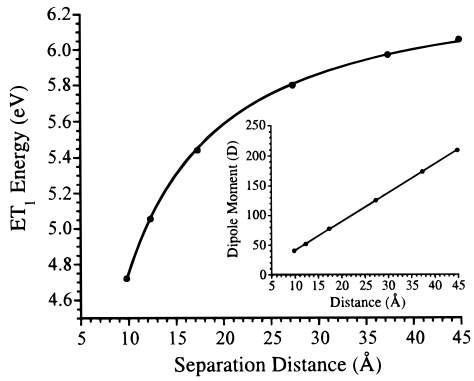


**Figure 7.** Plot of $ET_1$ energy versus the distance separating the pyrenyl and 1-methyl uracil subunits in six alkyl-linked compounds, PA−$(CH_2)_n$−$U_{Me}$, where $n = 2$, 4, 8, 16, 24, and 30. Distance was measured from the center of the pyrenyl ring to the center of the uracil ring. The six alkyl-linked compounds were derived from PA-$U_{Me}$ in that the linking NH-CO bond in PA-$U_{Me}$ was broken and varying numbers of methylene groups were inserted. For example, PA-$(CH_2)_4$−$U_{Me}$ was 5-(N-(4-carboxybutyl)-1-aminopyrenyl)-1-methyl uracil. Care was taken to retain the 1-aminopyrenyl and 5-carboxy uracil orientations in the alkyl-linked compounds as they were in PA-$U_{Me}$. Subject to this constraint, each alkyl-linked compound was PM3 geometry optimized before the CIS INDO/S computation of $ET_1$ state properties. The points were least squares fit to the equation $y = b - ax^{-1}$, $R = 0.9998$, and $b = 6.42(1)$ eV. The inset is a plot of the dipole moment of the $ET_1$ state versus the same pyrenyl/uracil distance as in the main plot. The inset points were least squares fit to a straight line: $R = 0.99996$, and the slope = 4.82 D/Å (or esu).

the distance data in Table 5 for *trans*- versus *cis*-conformers reveals much larger subunit separations for *trans*- compared to *cis*-conformers. If the least-squares correlation line for the *trans*-conformer data in Figure 6 is extrapolated to higher uracil LUMO energies, the data for the *cis*-conformers can be seen to lie below the extrapolated line. This energy difference (or deficit) is consistent with increased Coulombic stabilization between the cationic and anionic subunits in the ET products of *cis*-conformers compared to *trans*-conformers. Note that subunit separation distance (Coulombic energy) and CO/$U_{Me}$ dihedral angle (redox energy) contributions to the energy of the $ET_1$ state are independent of each other and can operate either in or out of phase with respect to varying the energy of the $ET_1$ state.

*Distance Dependence of ET Product Energies.* A natural question to ask concerning the CIS treatment of Coulombic effects on the energy ET products in pyrenyl−uracil conjugates is, "What is the distance dependence of this interaction?" A related concern is, "What is the limiting ET product energy at very large subunit separation?" To learn the answers to these questions, we carried out four different series of calculations. In each of them the pyrenyl and uracil subunit separations were varied. In one pair the subunits were spread apart between the 1-pyrenyl carbon and N-amide atoms, while in the other pair the subunits were spread apart between the N-amide and carbonyl carbon atoms of the linker. In each pair of computational series, the spreading of the subunits was done in two ways: (a) by inserting increasing numbers of methylene groups (a single molecule approach) and (b) by increasing distance alone (a bimolecular approach). In the latter case, the homolytically cleaved bonds in the original PA-$U_{Me}$ compound were terminated with methyl groups.

Figure 7 presents a plot of $ET_1$ energy versus subunit separation distance for the case of breaking the N-amide to carbonyl carbon bond of the linker in PA-$U_{Me}$ and inserting methylene groups, PA−$(CH_2)_n$−$U_{Me}$, where $n = 2$, 4, 8, 16, 24, and 30. The data fit an $x^{-1}$ function ($R = 0.9998$) as is expected for the distance dependence of the Coulombic energy of interaction between positive and negative point charges. This result is true also for the three other computational series investigated. The inset of Figure 7 presents a plot of the dipole moment of the $ET_1$ state versus subunit separation distance also for the PA−$(CH_2)_n$−$U_{Me}$ series. First, the fit of these data to a linear function is excellent ($R = 0.99996$). Second, the slope of this linear function (4.82 esu) agrees well with the charge of an electron (4.80 esu). Thus in the PA−$(CH_2)_n$−$U_{Me}$ series one electron is transfered from the pyrenyl HOMO to the uracil LUMO to form the $ET_1$ state, pyrene$^{\bullet+}$/dU$^{\bullet-}$. For the series in which the 1-pyrenyl carbon to the N-amide bond is broken and methylene groups are inserted, P-$(CH_2)_n$−$U_{Me}$, the $ET_1$ dipole moment versus subunit separation distance data fit a straight line with slope of 4.73 esu ($R = 0.9998$).

The fact that the data in Figure 7 for the PA−$(CH_2)_n$−$U_{Me}$ series fit an $x^{-1}$ function allows extrapolation of the $ET_1$ state energy to infinite separation between the pyrenyl and uracil subunits, 6.42(1) eV. Not surprisingly this is the value of the HOMO to LUMO gap in PA−$(CH_2)_n$−$U_{Me}$ molecules: e.g, for $n = 8$, the energy of the LUMO (−0.597 eV) minus the energy of the HOMO (−7.015 eV) is 6.418 eV. As a second example, when the methylene linker in this series of molecules is replaced with space (i.e., 1-aminomethylpyrene is separated from 5-acetyl-1-methyluracil), the extrapolated $ET_1$ state energy at infinite separation between the two molecules is 6.37 eV. The $R$ value for the $x^{-1}$ fit of the corresponding $ET_1$ energy versus separation distance data is 0.99999, and the HOMO to LUMO gap is 6.374 eV (= −0.648 + 7.022 eV).

Three facts emerge from the above studies on PA-$U_{Me}$ pyrenyl−uracil conjugates. (1) The extrapolated $ET_1$ energy agrees with that expected for an infinitely separated pyrene$^{\bullet+}$/$U_{Me}^{\bullet-}$ product within the Hartree−Fock approximation (Koopman's theorem).[36,37] (2) The amount of charge transferred to form the ET product corresponds to one electron at all separation distances excepting very short ones where charge delocalization across the subunits may occur. (3) The functional form of $ET_1$ energy variation versus ring-center-to-ring-center subunit separation is $x^{-1}$. It is thus inescapable that Coulombic attraction is the dominant interaction that lowers the $ET_1$ state energy as the cationic pyrenyl and anionic uracil subunits approach each other. Note that the above results and conclusions are unaffected by whether intervening methylene groups separate the pyrenyl and uracil subunits or only space separates them. Finally, Figure 7 shows that the $ET_1$ energy varies ca. 1.3 eV over the 10−45 Å range. Thus Coulombic stabilization is a significant factor in determining the energy of ET products in pyrenyl−dU nucleosides.

*Uracil LUMO Effects on $ET_1$ State Dipole Moments for the PA-$U_{Me}$ Model.* The above discussion establishes that two factors are important in determining the energy of the ET products in PMA-$U_{Me}$ conformers. The first is the ease of reduction of the uracil subunit as indicated by the energy of its LUMO. The second is the amount of Coulombic stabilization between the cationic and anionic subunits in the ET product. The dipole moment data in Table 5 show three trends. (1) There is significant variation of the $ET_1$ state dipole moment among PA−$U_{Me}$ conformers. (2) The dipole moments of the $ET_1$ states are much larger than are those of the corresponding lowest energy pyrenyl $(\pi,\pi^*)^1$ states. (3) The *cis*-conformer **E** has a larger pyrenyl $(\pi,\pi^*)^1$ state dipole moment than do any of the *trans*-conformers. The other two *cis*-conformers have pyrenyl $(\pi,\pi^*)^1$ state dipole moments of 4.6 and 7.4 D, also larger than the dipole moments of the $(\pi,\pi^*)^1$ states of all of the *trans*-conformers.

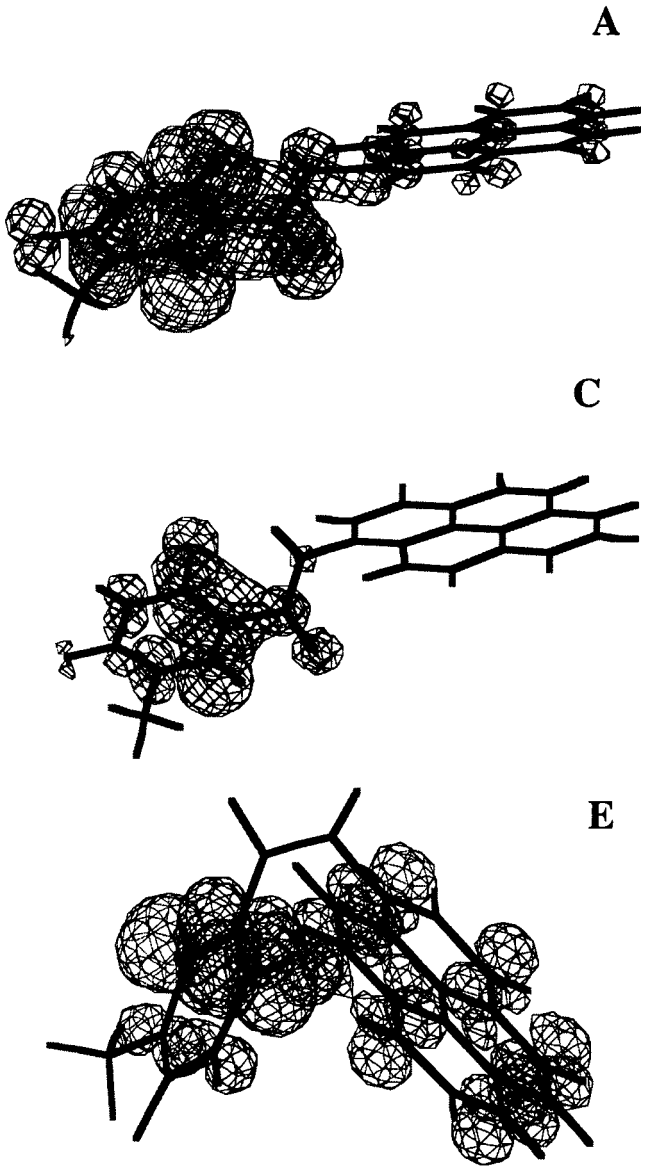


**Figure 8.** Plots of the Uracil LUMO for PA-$U_{Me}$ conformers **A**, **C**, and **E** in Table 5.

That ET products should have larger dipole moments than subunit localized excited states is expected. That the dipole moments of the lowest energy pyrenyl $(\pi,\pi^*)^1$ states for the *cis*-conformers are larger than are those for the *trans*-conformers implies that more ET character is mixed into the states of the *cis*-conformers than of the *trans*-conformers. Insight into the dipole moment variation among $ET_1$ states of PA-$U_{Me}$ conformers can come from examining their uracil LUMO shapes. Figure 8 presents plots of the uracil LUMO for conformers **A**, **C**, and **E**.

Although the CIS derived excited states do not arise solely from single HOMO to LUMO transitions, the nature and energy of the initial Hartree−Fock orbitals do exert strong effects on the final states. The effect of $CO/U_{Me}$ dihedral angle variation on $ET_1$ energy is an example of this phenomenon. Conformers **A**, **C**, and **E** have $ET_1$ state dipole moments, respectively, of 16.6, 28.5, and 23.5 D. Using the uracil LUMO as a measure of the spatial distribution of the highest energy electron in the $U_{Me}^{\bullet-}$ subunit suggests that the anionic charge in conformer **C** will be tightly concentrated on the C4−C5−C6 and linking carbonyl carbons. In contrast to **C**, the uracil LUMO of conformer A is more diffuse and has density extending well onto the pyrenyl subunit. Thus the $ET_1$ state of A should have a less charge separation than should the same state of C. Note that according to Table 5, **A** and **C** have similar subunit separation distances. The uracil LUMO for *cis*-conformer **E** has quite a different shape than it does for either of the *trans*-conformers **A** and **C**. Although in **E** the uracil LUMO extends onto the pyrenyl subunit as in **A**, it has no density on any of the linking amido atoms. The combination of these two effects yields and $ET_1$ dipole moment for **E** that is intermediate between those for **A** and **C** even though Table 5 shows that **E** has much smaller subunit separation distances than either **A** or **C**. For comparison recent CIS INDO/S computations on the closely related compound PMA-dU (see Figure 1) find that its *cis*-conformers have very little uracil LUMO density either on the linking atoms or on the pyrenyl subunit.[27] As a consequence five out of eight of the *cis*-PMA-dU conformers have $ET_1$ state dipole moments of 35−37 D. Thus the fact that the uracil LUMO extends onto the pyrenyl subunit in **E** reduces significantly the dipole moment of the $ET_1$ state relative to the situation in *cis*-PMA-dU compounds where this does not occur.

Figure 8 shows that the shapes of the uracil LUMO wavefunctions vary significantly among the different PA-$U_{Me}$ conformers and are far from uniformly distributed over the subunits. For example, the amido NH and CO bonds in conformer **A** are nearly coplanar with respect to their closest subunits (see Figure 4). This has consequence that the uracil LUMO extends onto both the NH and CO groups of the linker. In conformer **C** both of these bonds in the linker are nearly 45° out of the plane of their closest subunits. The consequence is that the uracil LUMO extends much less strongly on to the linking atoms than in conformer **A**. Finally, in conformer **E** the amido NH to pyrenyl C5−C4 dihedral angle is 59° and the $CO/U_{Me}$ angle is −84°. The consequence is that the uracil LUMO is totally absent from the linking atoms. Analysis of uracil LUMO shapes and their corresponding $ET_1$ properties in PA-$U_{Me}$ conformers suggests that the shapes of the specific HOMO and LUMO wave functions involved in forming a given excited state have a major influence on the resulting charge distribution in that state.

*Comparison of Electronic Spectra From CIS INDO/S Computations and Experiment for PA-Ac.* Figure 2 shows that the absorbance and emission spectra for PA-Ac are quite similar in THF, MeCN, and MeOH, although red-shifted in THF. Table 6 presents a comparison of the energies and oscillator strengths for the first seven singlet excited states of PA-Ac ($P_n$) obtained from CIS INDO/S computation with the three lowest energy (0,0) transitions observed for PA-Ac in MeCN: 384, 340, and 277 nm. Importantly, the semiempirical computation describes properly the dominant features of the absorbance spectrum of PA-Ac. A forbidden first excited singlet ($P_1$) and two well-spaced strongly allowed singlets. The assignments of the upper excited states of PA-Ac in Table 6 are arrived at by identifying the $P_2$ and $P_6$ states with large oscillator strength in the computations with the strong (0,0) absorbance features in the experimental spectrum. The first electronic transitions in both experiment and theory must coincide by definition. Having made these correspondences, Table 6 also shows that the computed state energies for PA-Ac are higher on average ($0.43 \pm 0.16$ eV) than are the state energies found in MeCN.

The excited states reported for PA-Ac in Table 6 ($P_{1-7}$) should also be present in the computations for PA-$U_{Me}$ and in the spectra for PA-dU. Comparison of the absorbance and emission spectra for PA-dU in Figure 3 with the corresponding spectra for PA-Ac in Figure 2 shows, however, that there are striking

**TABLE 6: Theoretical and Experimental Excited State Energies for PA-Ac**

| excited state | energy (eV) | oscillator strength | dipole moment (D) | $\Delta E$(theory-experiment) (eV)[a] |
|---|---|---|---|---|
| Gas Phase Computation[b] | | | | |
| $P_1$ | 3.72 | 0.027 | 4.53 | 0.45 |
| $P_2$ | 3.95 | 0.748 | 3.76 | 0.30 |
| $P_3$ | 4.09 | 0.006 | 1.40 | |
| $P_4$ | 4.54 | 0.002 | 4.58 | |
| $P_5$ | 5.03 | 0.021 | 4.23 | |
| $P_6$ | 5.07 | 0.791 | 5.56 | 0.54 |
| $P_7$ | 5.18 | 0.160 | 8.35 | |
| Experiment[c] | | | | |
| $P_1$ | 3.23 | very weak | | |
| $P_2$ | 3.65 | strong | | |
| $P_6$ | 4.48 | strong | | |

[a] Energy difference between the gas phase computational result and the (0,0) level of the corresponding electronic transition observed in UV−vis spectra. [b] CIS INDO/S single-point computation in HyperChem 5.1 using a PM3 optimized geometry.[32] [c] Data obtained from UV−vis absorbance and emission spectra for PA-Ac in MeCN solution (see Figure 2).

differences between the spectra of these two compounds. The next section will compare the computed excited states for PA-Ac with those for PA-$U_{Me}$ and will use the correspondence between these two excited-state manifolds to suggest why the spectra of PA-dU differ from the spectra of PA-Ac. This analysis will also show that the *cis*-conformers of PA-$U_{Me}$ have very different electronic spectra than do the *trans*-conformers. By way of referrence, it is worth noting that a similar spectral broadening in the absorbance spectrum of a D/A complex (relative to the isolated acceptor chromophore) was found for an ethylene linked complex comprised of donor *para*-methoxydimethylaniline and acceptor cyanoanthracene subunits.[39] The broadening in this case occurred only for the ethylene linked D/A complex and not for the methylene, propyl, or butyl linked complexes. It was ascribed to through-bond interaction of the D and A groups to form a ground state D/A complex that could be directly excited to its ET state.[39]

*Comparison of Electronic Spectra From CIS INDO/S Computations for PA-$U_{Me}$ and Experiment for PA-dU.* Table 7 presents a comparison of the energies and oscillator strengths obtained from CIS INDO/S computation for the first nine singlet excited states of PA-$U_{Me}$ conformers A and E with three strong low-energy absorbance bands and the $S_1(0,0)$ position observed for PA-dU in MeCN: 385, 358, 342, and 281 nm. The 385-nm $S_1(0,0)$ position is a shoulder on both the absorbance and emission spectra for PA-dU in MeCN as well as the vibrational origin for emission in MeOH (384 nm). The 358-nm band is the first absorbance maximum in the absorbance spectrum of PA-dU in MeCN, while the 342-nm band is a pronounced shoulder on the blue-side of the 358-nm band. The 281-nm band is strong and sharp. Since vibrational progressions are not seen in the absorbance spectrum for PA-dU, the (0,0) positions for electronic states above $S_1$ cannot be located with certainty.

The computational results for *trans*-PA-$U_{Me}$ conformer **A** in Table 7 show that nine, singlet excited states occur over the same 3.7−5.2 eV energy range in which only seven singlet states occur for PA-Ac. Inspection of the dipole moments for these nine lowest-energy singlet states of **A** shows that the two labeled $ET_1$ and $ET_2$ have significantly larger dipole moments than do those labeled $P_{1-7}$. Indeed the $ET_{1,2}$ electronic transitions have predominantly pyrenyl HOMO to uracil LUMO character. The states labeled $P_1$, $P_2$, and $P_6$ have obvious correspondence with the same states for PA-Ac in Table 6. One difference between

**TABLE 7: Comparison of Theoretical Excited State Energies for PA-$U_{Me}$ Conformers A and E With Experimental Energies for PA-dU**

| excited state | energy (eV) | oscillator strength | dipole moment (D) | $\Delta E$(theory−experiment) (eV)[a] |
|---|---|---|---|---|
| Gas Phase Computation for *trans*-PA-$U_{Me}$ Conformer **A**[b] | | | | |
| $P_1$ | 3.77 | 0.035 | 3.39 | 0.55 |
| $ET_1$ | 3.80 | 0.412 | 16.6 | 0.34 |
| $P_2$ | 4.02 | 0.464 | 5.11 | 0.39 |
| $P_3$ | 4.16 | 0.001 | 5.09 | |
| $P_4$ | 4.33 | 0.003 | 2.43 | |
| $P_5$ | 4.58 | 0.001 | 3.70 | |
| $ET_2$ | 4.76 | 0.058 | 18.9 | |
| $P_6$ | 5.01 | 0.912 | 1.43 | 0.60 |
| $P_7$ | 5.08 | 0.160 | 6.89 | |
| Gas Phase Computation for *cis*-PA-$U_{Me}$ Conformer **E**[b] | | | | |
| $P_1$ | 3.76 | 0.007 | 6.04 | 0.54 |
| $P_2$ | 3.98 | 0.617 | 7.77 | 0.35 |
| New/$P_3$ | 4.25 | 0.003 | 4.97 | |
| New/$P_3$ | 4.36 | 0.006 | 4.63 | |
| $ET_1$ | 4.42 | 0.082 | 23.5 | |
| $P_4$ | 4.62 | 0.002 | 5.65 | |
| $P_5$ | 5.05 | 0.017 | 6.90 | |
| $P_6$/$P_7$ | 5.13 | 0.212 | 7.13 | |
| $P_6$/$P_7$ | 5.17 | 0.932 | 8.53 | 0.76 |
| Experiment[c] | | | | |
| $P_1$ | 3.22[d] | very weak shoulder | | |
| 358 nm | 3.46 | strong broad maximum | | |
| $P_2$ | 3.63 | shoulder | | |
| $P_6$ | 4.41 | strong narrow band | | |

[a] Energy difference between the gas phase computational result and the absorbance maximum (or (0,0) level for $P_1$) of the corresponding electronic transition observed in UV-vis spectra. [b] CIS INDO/S single point computation in HyperChem 5.1 using a PM3 optimized geometry.[32] [c] Data obtained from UV−vis absorbance and emission spectra for PA-dU in MeCN solution (see Figure 2). [d] Measured halfway between the emission and absorbance origins.

them is that because in PA-$U_{Me}$ $ET_1$ is close to $P_2$ (3.80 and 4.02 eV, respectively), the $ET_1$ state has anomalous large oscillator strength (normally absorbance to ET states in pyrenyl−uracil conjugates is very weak),[27] and the $P_2$ state has reduced oscillator strength relative to PA-Ac. Note that in PA-$U_{Me}$ the sum of the oscillator strengths for the $ET_1$ and $P_2$ states is nearly the same as that of the $P_6$ state, and in PA-Ac the oscillator strengths of $P_2$ and $P_6$ are nearly the same. Although squeezing in new ET states in the pyrenyl manifold of singlet excited states could shift the energy of some of the pyrenyl states, only $P_4$ and $P_5$ are significantly perturbed (lowered in energy in PA-$U_{Me}$, respectively, 0.21 and 0.45 eV with respect to PA-Ac). The other five pyrenyl singlet states in PA-$U_{Me}$ are within ±0.10 eV of their energy in PA-Ac.

Three important conclusions arise from the CIS INDO/S computations for conformer **A**. First, the very strong pyrenyl absorbance to $P_2$ in PA-Ac is replaced in PA-$U_{Me}$ by two strong absorbances spread apart by ca. 0.22 eV. Second, a new strong absorbance band occurs in PA-$U_{Me}$ ca. 0.15 eV to the red of the $P_2$ band position in PA-Ac. Third the very strong absorbance to $P_6$ in PA-Ac remains, but red-shifts in PA-$U_{Me}$ ca. 0.06 eV. Applying these conclusions from calculations for PA-Ac and PA-$U_{Me}$ to the spectral observations for PA-Ac and PA-dU shows the following. Considering the third conclusion first, it is the true in MeCN that the $P_6$ absorbance band in PA-dU is 0.11 eV to the red of the $P_6$ absorbance band in PA-Ac. The observations that the very sharp $P_2$ absorbance band in PA-Ac is replaced by a much broader and red-shifted absorbance band in PA-dU is similarly in agreement with the above first and second conclusions from comparison of computational results.

Table 7 shows the excited-state assignments for the absorbance features identified above for PA-dU in MeCN. When the energies of these experimental bands are compared to their assigned calculated energies, the calculated energies are on average 0.47 ± 0.13 eV too high. This is the same offset that was found in the comparison of computational versus experimental energies for PA-Ac (0.43 ± 0.12 eV). The overall conclusions are that the type of absorbance spectrum calculated for PA-$U_{Me}$ conformer **A** agrees with that found for PA-dU, and furthermore the relative spectral differences calculated between PA-Ac and conformer **A** also agree with those found experimentally between PA-Ac and PA-dU. A corollary is that the strong absorbance in PA-dU at 358 nm could therefore be due to an ET transition that is borrowing oscillator strength from a strongly allowed pyrenyl excited state. It will be important to confirm these observations and conclusions with computations that include solvent/solute interactions.

Table 7 also presents PA-$U_{Me}$ computational results for the *cis*-PA-$U_{Me}$ conformer **E** over the same 3.7−5.2 eV energy range for which PA-Ac and *trans*-conformer **A** were investigated. Strikingly the computed absorbance spectrum for conformer **E** is remarkably similar to that for PA-Ac. In particular, both have forbidden $P_1$ states and two widely separated, strongly allowed P states ($P_2$ and $P_6$). Importantly, there are no new strongly allowed excited states below 5.2 eV that are not present in PA-Ac. This implies that the computed absorbance spectrum for PA-$U_{Me}$ *cis*-conformer **E** is inconsistent with the experimentally observed absorbance spectrum for PA-dU.

Details of the excited state structure of *cis*-PA-$U_{Me}$ conformer **E** are also interesting. Its $P_n$ states with $n = 1, 2, 5, 6$, and 7 have an average absolute value difference from the corresponding state in PA-Ac of only 0.03 ± 0.02 eV. $P_4$ is close to the $ET_1$ but is only 0.08 eV higher in energy than in PA-Ac. One surprise among the P states in conformer **E** is that the oscillator strengths of $P_6$ and $P_7$ are reversed relative to PA-Ac. However, these states are only 0.04 eV apart in conformer **E** but are 0.11 eV apart in PA-Ac. Apparently they are mixed with each other in conformer **E**. The $ET_1$ state in conformer **E** at 4.42 eV has a larger dipole moment (23.5 D) than either of the $ET_{1,2}$ states in conformer **A**. A second surprise in the excited-state manifold of conformer **E** is that two states appear in the $P_3$ region of PA-Ac, 4.09−4.36 eV, very close in energy to $ET_1$. These two states can be described as a mixture of a new PA-$U_{Me}$ transition with the previously identified $P_3$ pyrenyl transition of PA-Ac, hence the New/$P_3$ assignment for both states in Table 7. Note that both of these New/$P_3$ states are optically forbidden and have small dipole moments (4.97 and 4.63 D).

Inspection of the CIS INDO/S orbital transitions (i.e., the coefficients of the single excitation determinants) that give rise to the $P_3$ and New/$P_3$ electronic states, respectively, in PA-Ac and PA-$U_{Me}$ shows that these states have much in common. The $P_3$ state in PA-Ac arises from a dominant transition between bonding and antibonding orbitals that are localized exclusively on the bridging amido group. The New/$P_3$ state in PA-$U_{Me}$ at 4.25 eV (the lower energy of the two) has two a dominant orbital transitions. Both terminate in the same type of antibonding unoccupied molecular orbital (UMO) as does $P_3$ in PA-Ac, but they originate in two largely pyrenyl occupied molecular orbitals (OMOs) that also have extensive density on the bridging amido group. One has additional orbital density on both uracil carbonyl groups, while the other has additional density only on the C4-carbonyl of uracil. The small dipole moment for this state (4.97 D) reflects the fact that it has little shifting of charge between the pyrenyl and uracil subunits. The higher energy New/$P_3$ transition in PA-$U_{Me}$ at 4.36 eV involves orbital transitions located on the bridging amido group and on the uracil subunit. The single OMO from which it arises has density on the bridging amido group as well as on all carbonyl carbons and nitrogens of uracil. The UMO in which it terminates is an antibonding uracil type of orbital. Thus both of the New/$P_3$ transitions in PA-$U_{Me}$ lack pyrenyl-to-uracil ET character and involve orbitals with extensive density on the bridging amido group as does $P_3$ in PA-Ac. In contrast to $P_3$, however, the obital transitions that comprise the New/$P_3$ state also have significant density on the pyrenyl and uracil subunits.

## Discussion and Conclusions

**ET Product Lifetimes in PMA-dU.** Pyrene is an attractive chromophore to attach to DNA bases for the purposes of photoreducing or photooxidizing the attached base. It has a long-lived, lowest energy $(\pi,\pi^*)^1$ excited state (219 ns for PBA and 12 ns for PA-Ac in MeOH), and is reversibly oxidized and reduced. Thus it offers the possibility of highly efficient charge injection or extraction from an attached DNA base. A previous study of $P_{CO}$dU shows that indeed photoexcitation of pyrene produces (≤30 ps) the ET product pyrene$^{\bullet+}$/dU$^{\bullet-}$.[20] The problem is that the reverse ET to re-form the ground state of this pyrene-labeled nucleoside is exceeding fast (ca. 67 ps, 90% amplitude, for $P_{CO}$dU in MeOH). Thus the hope of using either the oxidized pyrene or reduced deoxyuridine species in this nucleoside as a sink for or source of electrons in studies of charge migration in DNA is low. One way of trapping the deoxyuridine anion would be to reduce the pyrene cation with a nearby donor in competition with reverse ET within the pyrene$^{\bullet+}$/dU$^{\bullet-}$ product. Thus slowing this reverse ET to ca. 0.5 ns is likely to be sufficient to trap a high yield of reduced deoxyuridine anions. The 500-nm emission data in Table 4 for PA-dU, $P_{CO}$dU,[19,20] and PMA-dU[27] in MeOH show that ET product emission is significantly longer for the PMA-dU than for the other two nucleosides. This shows that ET products live longer in PMA-dU than in either PA-dU or $P_{CO}$dU. Thus the emission lifetime results in Table 4 support two conclusions. One, inserting the −$CH_2$−NH− groups between the C5-uracil carbonyl and pyrenyl groups in $P_{CO}$dU to form PMA-dU slows the charge-recombination step in the latter nucleoside to the desired range. Two, inserting merely the −NH− group between the C5-uracil carbonyl and pyrenyl groups in $P_{CO}$dU to form PA-dU drastically shortens the charge recombination step.

It is likely that the ET product in PMA-dU lives longer than the one in $P_{CO}$dU because it is higher in energy relative to the ground state than the one in $P_{CO}$dU. If so, these two recombination reactions are examples of inverted ET in that more energetic charge recombinations are slower than less energetic ones.[27,40−44] Why then is the charge recombination step within the ET product of PA-dU so fast (as evidenced in Table 3 by the ultrashort emission lifetimes in the 500−600 nm range for MeOH)? A contributing factor is that the $ET_1$ state in PA-dU is likely to be lower in energy than in $P_{CO}$dU and PMA-dU. Note that the 1-aminopyrenyl subunit in PA-dU should be easier to oxidize than the pyrenyl subunits in PMA-dU and $P_{CO}$dU (conclusion supported by PM3 calculations showing a 0.2 eV greater ease of oxidizing (*N*-methyl)-1-aminopyrene versus 1-methyl pyrene). Also, the CIS INDO/S range of $ET_1$ energies for PA-$U_{Me}$ is 3.80−4.42 eV, while that for PMA-$U_{Me}$ is higher, 3.94-4.82.[27] Thus the $ET_1$ state for PA-dU should have the shortest charge recombination lifetime among these three nucleosides, again consistent with inverted reactions. The progressively shorter emission lifetime of the pyrenyl $(\pi,\pi^*)^1$

state of PA-dU in the solvent series THF, MeCN, and MeOH (see Table 3) is likely due to increasingly fast ET emission quenching as the $ET_1$ state drops in energy with increasing solvent polarity and proton donating ability.

***cis*- and *trans*-Conformers in the PA-$U_{Me}$ Model.** For all three of the PA-dU, $P_{CO}$dU, and PMA-dU nucleosides, multiexponential ($\pi,\pi^*$)[1] emission decays were observed in all three solvents studied, THF, MeCN, and MeOH. For PA-dU two lifetimes were required in THF and three in MeCN and MeOH. Clearly knowing the factors that control the energetics of the lowest energy ET state in PA-dU is key to understanding its complicated emission decays. In this study PM3 semiempirical conformer-search computations were performed on the PA-$U_{Me}$ model to learn about likely pyrenyl−uracil ground-state geometries. Then CIS INDO/S single-point excited-state computations were performed on each of the eleven conformers found in the search to learn about the energy range of their $ET_1$ states and about the factors that controlled this energy variation. Thus vertical ET product energies were computed at the ground state conformer equilibrium geometries, and solvent effects were neglected. The resulting PMA-$U_{Me}$ conformers fell into *cis*- and *trans*-amide families.

Semiclassical ET theory shows that ET rates depend not only on the free energy of the reaction, but also on the electronic coupling and on the reorganization energy ($\lambda$) of the reaction.[40,41,43] While the reorganization energy for a series of PA-dU (or PA-$U_{Me}$) conformers is likely to be similar, the same is not necessarily true for their electronic coupling. We have not investigated the range of electronic coupling in the PMA-$U_{Me}$ conformer models, and we have no estimate of the range of its variation. To the extent the coupling is strong enough to be near the adiabatic limit, the ET rate for pyrene* quenching will be controlled by nuclear motions and not by the electronic coupling. Because the uracil LUMO extends onto both the bridge and the pyrenyl subunit for the *trans*-conformers and onto the pyrenyl subunit for the *cis*-conformers, it is likely that all PA-$U_{Me}$ conformers may be at or above the adiabatic limit. The quantum mechanical computations presented in this study are directed at determining likely ground state pyrenyl−uracil conformations and the range of their $ET_1$ state vertical energies in the gas phase.

Only indirect information exists as to whether both *cis*- and *trans*-conformers of PA-Ac and PA-dU are present in this study. However, the pattern of emission decay amplitudes and lifetimes as solvent is varied in the series THF, MeCN, and MeOH (see Table 3) does not suggest constant fractions of two different classes of conformers. Also, the energy variation of the ET product states within the *trans*-family of conformers (ca. 0.5 eV) seems large enough to account for the wide variation of pyrene* ET quenching lifetimes (380−440 nm emission). NMR evidence suggests that PA-Ac exists only as the *trans*-conformer. A typical barrier to rotation about the amido C−N bond is on the order of 20 kcal/mol due to its partial double bond character.[31] Thus *cis*- and *trans*-nitrogen substituents experience different environments and each can usually be observed by NMR well above room temperature.[31] The $^1$H spectrum of PA-Ac shows only a single strong, sharp *N*-methyl peak; thus it is very likely due to a single amide conformer. Additionally in N-monosubstituted amides, the *trans*-conformation is strongly preferred over the *cis*-conformation.[31] Importantly in both the gas and condensed phases only the *trans*-conformer of *N*-methylacetamide is found, while in crystallographic studies both *N*-methylacetamide and *N*-phenylacetamide have the *trans*-conformation.[31] These results imply that PA-Ac exists solely as the *trans*-conformer. Because steric considerations play such an important role in determining the conformation of N-monosubstituted amides, it is likely that PA-dU exists only as the *trans*-conformer also. In the *trans*-geometry the N-pyrenyl and C-uracil substituents of the amido group will be farthest apart. This is similar to the situation for N-monoalkyl and C-alkyl amides where only *trans*-conformers are found.[31]

Gas-phase computations of the absorbance spectra for PA-$U_{Me}$ are also consistent with the conclusion that PA-dU exists only as *trans*-conformers. Four out of the eight *trans*-conformers found for PA-$U_{Me}$ have absorbance spectra that resemble the absorbance spectra of PA-dU in solution. The other four *trans*-conformers and all three *cis*-conformers have absorbance spectra that resemble that of PA-Ac and not that of PA-dU. The key factor determining which type of spectrum a conformer has is the location of its $ET_1$ state. The four *trans*-conformers that have absorbance spectra like that of PA-dU have lower $ET_1$ energies (3.80−4.07 eV), while the other *trans*- and all of the *cis*-conformers that do not have such spectra have a higher $ET_1$ energy (4.17−4.42 eV). If the $ET_1$ state's energy is too high, it cannot mix with the lower energy $P_{1-3}$ excited states. Unless an ET state mixes with the $P_{1-3}$ states, a strong broad absorbance in the $P_{1,2}$ region of the spectrum cannot occur. Importantly, because the *cis*-conformers of PA-$U_{Me}$ have CO/$U_{Me}$ dihedral angles that are nearly perpendicular to the uracil plane, they also have high energy uracil LUMOs (see Figure 5) and high energy $ET_1$ states (see Figure 6). Thus their absorbance spectra resemble that PA-Ac and not that of PA-dU.

The general conclusion from the PA-$U_{Me}$ gas phase computations concerning the requirement to have at least one low energy ET state in the $P_{1-3}$ region in order to produce an absorbance spectrum resembling that of PA-dU will remain true in CIS computations that include solvent/solute interactions. However, which conformers will meet this requirement in solution phase computations cannot be guessed. The reason is that while ET states can drop in energy upon solution in a polar solvent, their degree of stabilization depends on the size of each state's dipole moment and a state's dipole moment in solution is not the same as it is in the gas phase. This work shows, however, that PA-dU and PA-Ac constitute an interesting system for future computational study of solvent/solute effects on intramolecular ET.

*ET Product Energies in the PMA-$U_{Me}$ Model.* CIS INDO/S computations for the PMA-$U_{Me}$ model show that two factors are major contributors to the variation in ET product energies among the eleven PA-$U_{Me}$ conformers identified. The first is the energy of the uracil LUMO, and the second is the pyrene/$U_{Me}$ separation distance. The energy of the uracil LUMO reflects the ease of reduction of the uracil subunit with lower energies corresponding to greater ease of reduction. Clearly making the $U_{Me}$ subunit easier to reduce lowers the energy of a pyrene$^{\bullet+}$/$U_{Me}^{\bullet-}$ ET product. Importantly, the dihedral angle between the bridging carbonyl and the C5−C4 bond in $U_{Me}$ is strongly correlated ($R = 0.94$, see Figure 5) with the energy of the uracil LUMO. This correlation is the major reason why the ET product energies are higher for *cis*- than for *trans*-conformers: the absolute value of the CO/$U_{Me}$ dihedral angle is 84−98° for the *cis*-conformers (nearly a right angle with respect the uracil plane) and 130−170° for the *trans*-conformers (approaching the uracil plane).

The second factor that contributes to the variation in ET product energies in the PMA-$U_{Me}$ conformers is the separation distance of the cationic and anionic subunits. This is easily understood as reflecting the fact that those conformers with

closely spaced cationic and anionic subunits experience larger Coulombic stabilization of their ET products than do those conformers with wide subunit separations. Quantitative study of the energy of the $ET_1$ state versus pyrenyl−uracil separation distance for two positions of breaks in the linking bond of PA-$U_{Me}$ shows a smooth $x^{-1}$ increase in $ET_1$ energy as the separation distance increases. Additionally, the extrapolated $ET_1$ energy at infinite subunit separation equals the difference between the Hartree−Fock LUMO and HOMO energies.

Variation of either the pyrenyl LUMO's energy or the pyrenyl/uracil electronic coupling with conformational change is not desirable for single-step charge injection into a DNA duplex. This work suggests that linking pyrenyl and uracil subunits via a carbonyl attached to the uracil C5-position makes the ET product energies of such conjugates sensitive to the relative geometries of the subunits as well as of the linking groups. Such geometry-dependent ET product energy variations should be minimized in new pyrenyl−deoxyuridine nucleosides developed to produce long-lived ET products.

**Acknowledgment.** This work was supported at Georgia State University and Washington State University by a Grant to T.L.N. and B.E.E. from the United States National Science Foundation (Grant NSF-CHE-9709318). T.L.N. thanks Marla Netzel for invaluable library research assistance.

## References and Notes

(1) Netzel, T. L. A Comparison of Theoretical and Experimental Studies of Electron-Transfer within DNA Duplexes. In *Organic and Inorganic Photochemistry*; Ramamurthy, V., Schanze, K. S., Eds.; Molecular and Supramolecular Photochemistry Series 2; Marcel Dekker: New York, 1998; pp 1−54.

(2) Barbara, P. F.; Olson, E. J. J. *Adv. Chem. Phys.* **1999**, *107*, 647−676.

(3) Barton, J. K. *Pure Appl. Chem.* **1998**, *70*, 873−879.

(4) Giese, B.; Wessely, S.; Spormann, M.; Lindemann, U.; Meggers, E.; Michel-Beyerle, M. E. *Angew. Chem., Int. Ed. Engl.* **1999**, *38*, 996−997.

(5) Meggers, E.; Michel-Beyerle, M. E.; Giese, B. *J. Am. Chem. Soc.* **1998**, *120*, 12950−12955.

(6) Harriman, A. *Angew. Chem., Int. Ed. Engl.* **1999**, *38*, 945−949.

(7) Fukui, K.; Tanaka, K. *Angew. Chem., Int. Ed. Engl.* **1998**, *37*, 158−161.

(8) Lewis, F. D.; Wu, T.; Zhang, Y.; Letsinger, R. L.; Greenfield, S. R.; Wasielewski, M. R. *Science* **1997**, *277*, 673−676.

(9) Ratner, M. *Nature* **1999**, *397*, 480−481.

(10) Jortner, J.; Bixon, M.; Langenbacher, T.; Michel-Beyerle, M. E. *Proc. Natl. Acad. Sci. U.S.A.* **1998**, *95*, 12759−12765.

(11) Kelley, S. O.; Barton, J. K. *Science* **1999**, *283*, 375−381.

(12) Kelley, S. O.; Jackson, N. M.; Hill, M. G.; Barton, J. K. *Angew. Chem., Int. Ed. Engl.* **1999**, *38*, 941−944.

(13) Kelley, S. O.; Barton, J. K. *Chem. Biol.* **1998**, *5*, 413−425.

(14) Franklin, S. J.; Treadway, C. R.; Barton, J. K. *Inorg. Chem.* **1998**, *37*, 5198−5210.

(15) Dandliker, P. J.; Holmlin, R. E.; Barton, J. K. *Science* **1997**, *275*, 1465−1468.

(16) Stemp, E. D. A.; Arkin, M. R.; Barton, J. K. *J. Am. Chem. Soc.* **1997**, *119*, 2921−2925.

(17) Ly, D.; Sanii, L.; Schuster, G. B. *J. Am. Chem. Soc.* **1999**, *121*, 9400−9410.

(18) Netzel, T. L. NSF Progress Report, Aug. '98 − July '99. U. S. National Science Foundation: Washington, DC, 1999; Report CHE-9709318.

(19) Netzel, T. L.; Zhao, M.; Nafisi, K.; Headrick, J.; Sigman, M. S.; Eaton, B. E. *J. Am. Chem. Soc.* **1995**, *117*, 9119−9128.

(20) Netzel, T. L.; Nafisi, K.; Headrick, J.; Eaton, B. E. *J. Phys. Chem.* **1995**, *99*, 17948−17955.

(21) Dewey, T. M.; Zyzniewski, M. C.; Eaton, B. E. *Nucleosides & Nucleotides* **1996**, *15*, 1611−1617.

(22) Wahlstrom, J. L.; Ronald, R. C. *J. Org. Chem.* **1998**, *63*, 6021−6022.

(23) Lakowicz, J. R. *Principles of Fluorescence Spectroscopy*; Plenum Press: New York, 1986.

(24) Parker, C. A.; Rees, W. T. *Analyst (London)* **1960**, *85*, 587.

(25) Demas, J. N.; Crosby, G. A. *J. Phys. Chem.* **1971**, *75*, 991−1024.

(26) Berman, H. M.; Young, P. R. *Annu. Rev. Biophys. Bioeng.* **1981**, *10*, 87−114.

(27) Kerr, C. E.; Michell, C. D.; Ying, Y.-M.; Eaton, B. E.; Netzel, T. L. *J. Phys. Chem. B* **2000**, *104*. Submitted for publication.

(28) Stewart, J. J. P. *J. Comput. Chem.* **1989**, *10*, 209−220.

(29) Stewart, J. J. P. *J. Comput. Chem.* **1989**, *10*, 221−264.

(30) Spartan version 5.1.1; Wavefunction, Inc.: 18401 Von Karman Avenue, Suite 370, Irvine, CA 92612.

(31) Robin, M. B.; Bovey, F. A.; Basch, H. Molecular and Electronic Structure of the Amide Group. In *The Chemistry of Amides*; Zabicky, J., ed.; The Chemistry of Functional Groups; Wiley-Interscience Publishers: New York, 1970; pp 1−72.

(32) *HyperChem, version 5.1*; Hypercube, Inc.: 419 Phillip Street, Waterloo, Ontario N2L 3X2, Canada.

(33) Foresman, J. B.; Head-Gordon, M.; Pople, J. A.; Frisch, M. J. *J. Phys. Chem.* **1992**, *96*, 135−149.

(34) Zerner, M. C. Semiempirical Molecular Orbital Methods. In *Reviews in Computational Chemistry II*; Libkowitz, K. B., Boyd, D. B., Eds.; VCH Publisher: New York, 1991; Chapter 8, 313−366.

(35) Zerner, M. C.; Loew, G. H.; Kirchner, R. F.; Mueller-Westerhoff, U. T. *J. Am. Chem. Soc.* **1980**, *102*, 589−599.

(36) Ridley, J.; Zerner, M. C. *Theor. Chim. Acta (Berlin)* **1973**, *32*, 111−134.

(37) Koopmans, v. T. *Physica* **1934**, *1*, 104−113.

(38) Sevilla, M. D.; Besler, B.; Colson, A. O. *J. Phys. Chem.* **1995**, *99*, 1060−1063.

(39) Yang, N. C.; Zhang, S.-L.; Lang, M. J.; Goodman, S.; Durnell, C.; Fleming, G. R.; Carrell, H. L.; Garavito, R. M. *Adv. Chem. Phys.* **1999**, *106*, 645−666.

(40) Brunschwig, B. S.; Ehrenson, S.; Sutin, N. *J. Phys. Chem.* **1986**, *90*, 3657−3688.

(41) Sutin, N. Nuclear and Electronic Factors in Electron Transfer: Distance Dependence of Electron-Transfer Rates. In *Electron Transfer in Inorganic, Organic, and Biological Systems*; Bolton, J. R., Mataga, N., McLendon, G., Eds.; Advances in Chemistry Series 228; American Chemical Society: Washington, DC, 1991; pp 25−43.

(42) Marcus, R. A. *J. Chem. Phys.* **1956**, *24*, 966−978.

(43) Marcus, R. A.; Sutin, N. *Biochim. Biophys. Acta* **1985**, *811*, 265−322.

(44) Marcus, R. A. *Science* **1992**, *256*, 1523−1524.